

東京大学大学院新領域創成科学研究科

複雑理工学専攻

令和5年度

修士論文

**Performance evaluation of Kashiwa ground station for  
satellite operation**

2023年09月01日提出

指導教員 吉川 一朗 教授

張 梦彤

# **Performance evaluation of Kashiwa ground station for satellite operation**

**Zhang Mengtong**

47-216144

Complexity Science and Engineering

Completed: September 2023

Keywords: *X-Y Antenna, Ground station, LEO Satellite, Autonomous tracking system,*

*True north calibration, Power Pattern, G/T*

## **Abstract**

Artificial satellites are currently becoming smaller thanks to advancements in semiconductor technology, making it possible to produce and launch them more swiftly and affordably. As a result, the number of satellite launches has continued to skyrocket in recent years. To exchange data and commands and establish communication with thousands of satellites, radio waves are used to broadcast and receive signals via satellite ground stations. The ground station's performance metrics directly impact the satellite signal's ability to transmit and receive data. Since it is essential to ensure the stability, dependability, and effectiveness of satellite communications and data transfer, it is necessary to understand the unique performance criteria of a ground station to evaluate its capacity to adapt to different communication needs. The major objective of this study was to investigate the performance of Kashiwa ground station. Expressly, an in-depth understanding of constructing a highly automated ground station is provided, and the true north calibration, power pattern, and G/T are discussed.

# Contents

<i>Acknowledgement</i> .....	<i>1</i>
<i>1. Introduction</i> .....	<i>2</i>
<b>1.1 Background</b> .....	<b>2</b>
<b>1.2 Kashiwa ground station</b> .....	<b>5</b>
<b>1.3 Purpose and Overview</b> .....	<b>7</b>
<i>2. Fundamental technologies for Kashiwa ground station</i> .....	<i>8</i>
<b>2.1 Hardware configurations</b> .....	<b>8</b>
2.1.1 Overview.....	8
2.1.2 X-Y type Antenna .....	9
<b>2.2 Software systems</b> .....	<b>14</b>
2.2.1 Overview.....	14
2.2.2 Antenna control subsystem .....	15
2.2.3 Tracking receiver subsystem.....	26
2.2.4 Digital demodulator subsystem.....	30
<b>2.3 Satellite tracking technology</b> .....	<b>31</b>
2.3.1 Satellite position calculation .....	31
2.3.2 Real-time automatic tracking method .....	40
<i>3. Performance evaluation for Kashiwa ground station</i> .....	<i>43</i>
<b>3.1 True north calibration</b> .....	<b>43</b>
3.1.1 Description.....	43
3.1.2 Measurement method.....	44

<b>3.2 Power pattern .....</b>	<b>45</b>
3.2.1 Description .....	45
3.2.2 Measurement method .....	47
<b>3.3 G/T (Gain to Noise Temperature) .....</b>	<b>49</b>
3.3.1 Description .....	49
3.3.2 Measurement method .....	52
<b>4. Results and Discussions .....</b>	<b>58</b>
<b>4.1 True north calibration .....</b>	<b>58</b>
<b>4.2 Power pattern .....</b>	<b>59</b>
<b>4.3 G/T (Gain to Noise Temperature) .....</b>	<b>61</b>
<b>5. Summary .....</b>	<b>67</b>
<b>Reference.....</b>	<b>69</b>

# Acknowledgement

First and foremost, I would like to express my sincere gratitude to Prof. Ichiro Yoshikawa for his helpful recommendations and astute observations.

Additionally, I want to thank Dr. Yokotsuka of Astorocub (formerly of Tokai University) for his candid responses to my inquiries about the setup of the antenna system.

I also want to express my gratitude to Prof. Takeshi Imamura and Lecturer Dr. Kazuo Yoshioka for their advice and insightful comments.

Thank you to my Yoshikawa lab mates: Mr. Yi Yang, Mr. Huiyang Lin, Mr. Masato Sasaki, Mr. Xuanchao Fu, Mr. Wenhao Shen, Ms. Shuyue Liu, and Mr. Shunichiro Teramoto for the thought-provoking conversations and all the knowledge we have acquired over the past two years.

In closing but not least, I would like to thank my parents and friends for their support during my master's class.

# **1. Introduction**

## **1.1 Background**

With advances in semiconductor technology, electronic devices have become smaller and lighter. The tiny size of integrated circuits and chips allows for more compact device designs, enabling higher levels of integration and more functionality, making it more feasible and affordable to build smaller satellites and reducing launch costs.

In addition, communication and the Internet have become basic needs of modern society, and people need fast and reliable communication channels and extensive Internet coverage. Satellite communication technology provides a solution for global communication over a wide geographical area and is particularly important for remote areas and maritime domains. On the other hand, satellite navigation systems (such as GPS) not only provide high accuracy and reliability for navigation, but are also widely used in transportation, aviation, military, and other fields, becoming an indispensable part of modern society.

At the same time, high-precision image processing and measurement technologies are increasingly important for applications such as scientific surveying, resource management, and environmental monitoring. The advanced sensors onboard satellites can acquire high-resolution images of the Earth's surface, providing important geographic and environmental information. These data are important for climate change research, natural disaster monitoring, agricultural management, and other fields. As a result, there is a growing demand from the scientific community and government

agencies for satellite launches and the establishment of Earth observation satellite networks.

Main purpose	2020.12.31	2021.12.31	increase
Communications purpose	1832	3135	1303
Earth Observation	906	1030	124
Technology development and demonstration	350	385	35
Navigation and positioning	150	154	4
Space science and observation	104	108	4
Earth science	20	22	2
Other purposes	10	18	8

**Table 1.1 The increase in the number of artificial satellites in orbit during 2021**

As in Table 1.1, in 2021, there were 1303 more communication satellites, 124 more Earth observation satellites, and 53 more satellites for other uses. According to the data, the demand for satellites has dramatically increased in today's society. However, there is a significant issue which is the time limit for communication with satellites.

The ground station can interact with the satellite only when the satellite passes directly above the ground station (called a pass). Figure 1.1 shows the vertical projection of a polar orbiting satellite trajectory onto the surface of the Earth. It can be observed that the ground projection trajectory is shifted from side to side, and the time interval between adjacent projection points at the same latitude (roughly equal to the time

interval between two passes) is approximately equal to one orbital period. Especially in the high latitude area circled in red, there will be more passes per day.

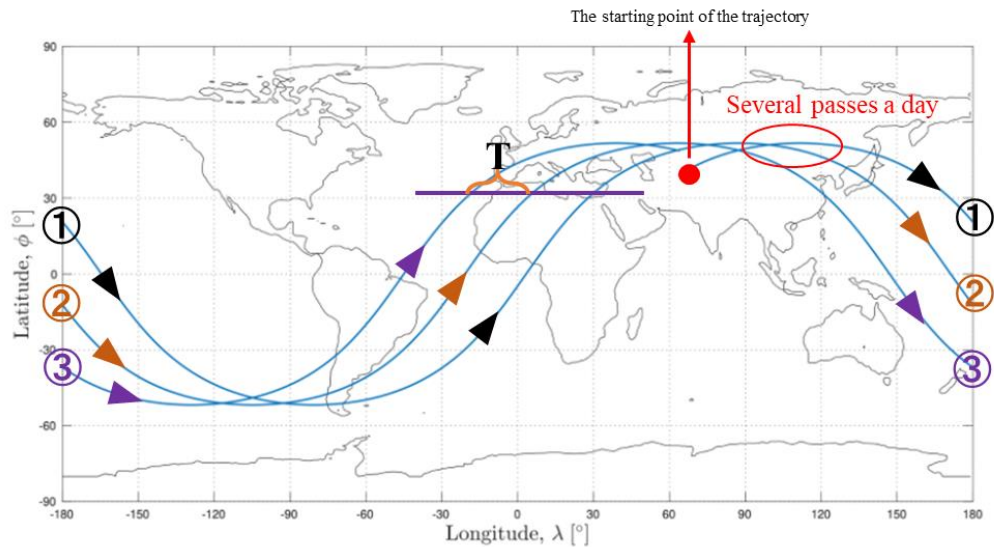


**Figure 1.1 Ground tracks: the vertical projection of the satellite's orbit onto the surface of the Earth**

The duration of a pass is determined by the satellite's orbit, and generally, a pass from a low earth orbiting satellite will last for about 10 minutes. Table 1.2 shows the daily time of total passes with the polar orbiting satellite at different latitudes. The higher the latitude, the longer the total communication time, so certain satellites (such as Terra) will transmit large amounts of stored data in polar regions.

Latitude (degrees)	80	70	60	50	40	30	20	10	0
Number of passes per day	13	10	9	6	5	4	4	3	3
The time of total passes per day (minutes)	150	115	89	59	47	40	37	35	34

**Table 1.2 Communication time with the polar-orbiting satellite**

Artificial satellites have the advantage of being able to communicate remotely and

obtain information globally, but they also have the disadvantage of only being able to exchange data for a limited and short period of time each day, resulting in a large amount of satellite data not being available and utilized in a timely manner. To make more efficient use of satellite data resources, there is a need to build lower-cost, highly automated ground stations to manage and receive satellite signals. This trend reflects a shift in the understanding of the space enterprise from state-led "space development" to private-sector-led "space utilization," which implies an increase in the participation of individuals and organizations in the application and development of satellite technology.

## **1.2 Kashiwa ground station**

Kashiwa ground station has two X-band antennas and one S-band antenna for acquiring continuous high-resolution images of the Earth's surface from the many satellites orbiting the Earth. The goal is to apply artificial intelligence technology to satellite operations to establish an efficient and autonomous ground station (Smart Ground Station; Smart GS) for global measurements.

Smart GS is a system that efficiently analyzes the large amount of data received from satellites and makes sense of the information acquired. The system is capable of automatically generating the following observation request and planning the next satellite operation plan instantly for efficient satellite operations. Figure 1.2 shows the detailed schematic diagram of data processing system at Smart GS. In this Smart GS project, the highly automated ground station system construction was assisted by Astrocub Inc., and the image recognition and disaster detection technology using AI was researched and developed by National Institute of Advanced Industrial Science and

Technology (AIST).

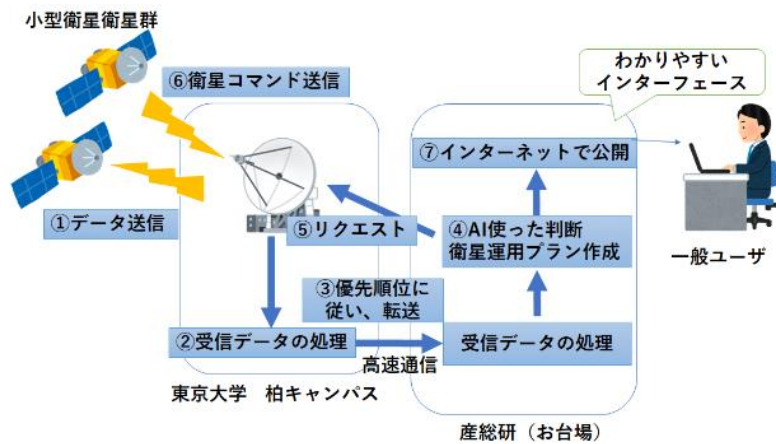


**Figure 1.2 Schematic diagram of data processing system at Smart GS**

In addition, the Kashiwa ground station will be operating the satellite in conjunction with other ground stations. As shown in Figure 1.3, with multiple ground stations working in tandem, the satellite side needs to modify its transceiver parameters in response to the performance of the various ground stations in order to ensure highly accurate data transmission. Due to the project's rapid progress, the performance of the Kashiwa ground stations is still unknown in some respects, and therefore their performance needs to be accurately obtained.

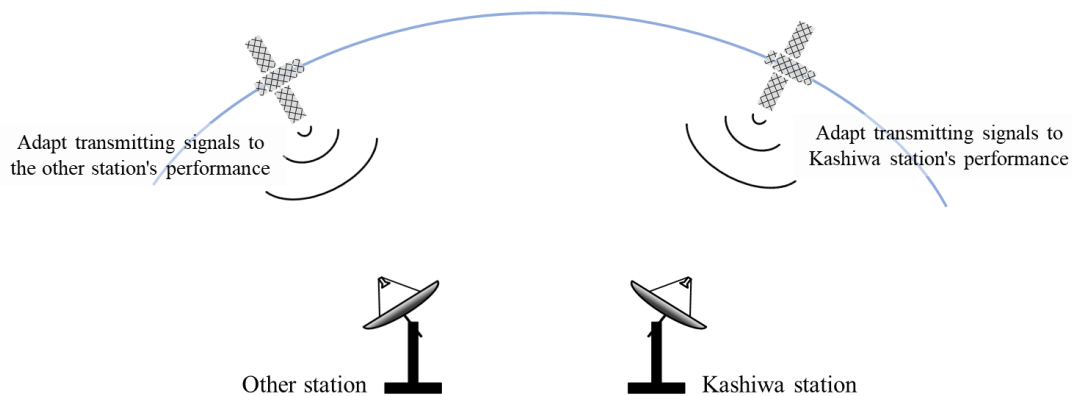


**Figure 1.3 Conceptual diagram of a joint operation with other ground station**

### **1.3 Purpose and Overview**

In the foreseeable future, the Kashiwa station will jointly operate a satellite with the Taiwan station. We need to ensure accurate data communication and plan the operation by precisely identifying the characteristics of each ground station. In this study, we provide an in-depth understanding of the system components of an autonomous ground station and evaluate the performance of the Kashiwa ground station to ensure the reliability and quality of received data during satellite operations.

This thesis will focus on the system components of the Kashiwa ground station and its performance evaluation:

In Chapter 2, the fundamental technologies for the Kashiwa ground station are introduced and discussed in detail. This section comprises hardware configurations, software systems, and satellite tracking technology.

In Chapter 3, the performance indexes of Kashiwa ground station and its measurement methods are introduced, mainly discussing the true north calibration, the power pattern of the antenna, and the G/T of the antenna receiving system.

In Chapter 4, the measurement results and their discussion are shown.

In Chapter 5, we will provide our conclusion and describe future issues.

## 2. Fundamental technologies for Kashiwa ground station

### 2.1 Hardware configurations

#### 2.1.1 Overview

The Kashiwa ground station is now only used to receive satellite signals in S-band (2 - 4 GHz) and X-band (8 - 12 GHz). Figure 2.1 shows the hardware configuration of the Kashiwa ground station's antenna reception system.

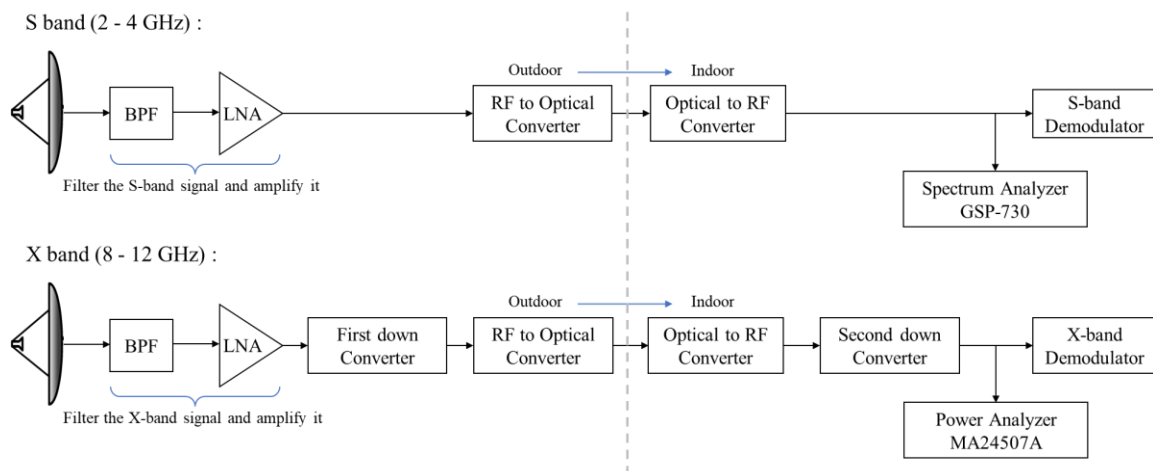


**Figure 2.1 The hardware configuration of the Kashiwa ground station's antenna reception system**

As shown in Figure 2.1, in the S-band antenna reception system, the signal is transmitted through the parabolic antenna, band-pass filter, and low-noise amplifier to filter out the signal other than the target frequency. A spectrum analyzer (GSP-730) is used to monitor whether the satellite signal was adequately received and record the signal strength before the demodulation. In the X-band antenna reception system, the signal is downconverted 6 GHz outdoors before being transmitted indoors and is

secondly downconverted before the demodulation. Here the satellite signal is monitored and recorded using a power analyzer (MA24507A).

### 2.1.2 X-Y type Antenna

The antenna of the Kashiwa ground station is an X-Y type antenna with a 2.4m parabolic reflector manufactured by Astrocub Inc. (Figure 2.2).

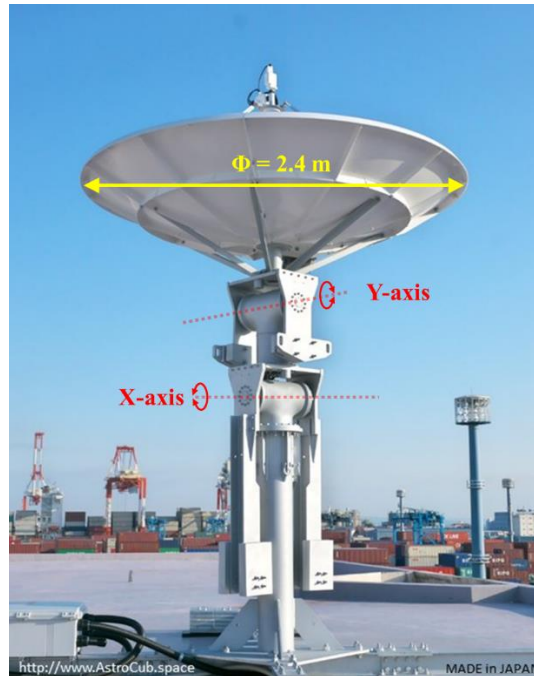


**Figure 2.2 The X-Y type Antenna used in the Kashiwa ground station**

X-Y type antenna is one of the two-axis antennas commonly used in low-cost ground stations. Two-axis antenna mount with orthogonal axes is the most straightforward configuration capable of pointing an antenna at any position in the sky. Figure 2.3 shows two types of two-axis antenna mounts.

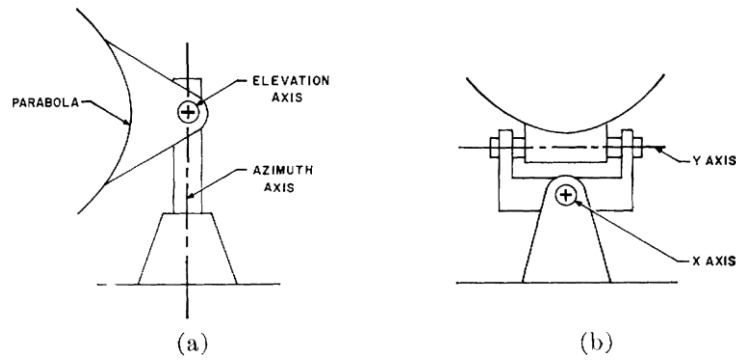


**Figure 2.3 Two-axis antenna mount types: (a) Az-El mount (b) X-Y mount  
( Rolinski et al., 1962 )**

As shown in Figure 2.3 (a), the Azimuth-Elevation(Az-El) mount has a vertical Az axis with a rotation range of  $0^{\circ}$ - $360^{\circ}$  and a horizontal El axis with a rotation range of  $0$ - $90$  degrees. Figure 2.3 (b) shows the axial arrangement of the X-Y mount. The X-axis and Y-axis each have a rotational range of  $0^{\circ}$ - $180^{\circ}$ .

However, the drawback of the two-axis antenna is that it has some blind zones where it is impossible to follow a satellite. It occurs in those areas where one of the axes of the antenna must rotate by a large angle, even when there is just a slight movement in space (As Figure 2.4). Therefore, when tracking satellites with a certain speed in these areas, the maximum axis speed limits the movement of the antenna, making it impossible to align the antenna accurately with the satellite in this area.

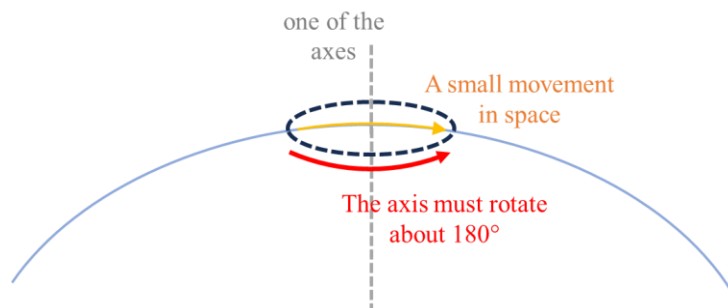


**Figure 2.4 Two-axis antenna blind zone occurrence reason**

For the Az-El mount, the blind zone occurs in the area of the sky around the zenith (El around  $90^\circ$ ), where a slight pointing offset can cause a great rotation of the Az axis. And for the X-Y mount, the blind zone occurs in the area around  $0^\circ$  and  $180^\circ$  of the Y-axis, where a slight pointing offset will result in a great rotation of the X-axis. If the X-Y axis angle is converted to the geographic Az-El angle (the conversion method will be covered in the following content), the X-Y mount antenna will have a blind zone in the low elevation angle region ( $EL < 6^\circ$ ) where Az is  $0^\circ$  (north) and  $180^\circ$  (south). Figure 2.5 shows the simulation of the X-axis rotation speed while scanning azimuth angles in the range of  $0^\circ$ - $360^\circ$  at a speed of  $0.1^\circ/\text{s}$  when the elevation angle is fixed at  $3^\circ$ .

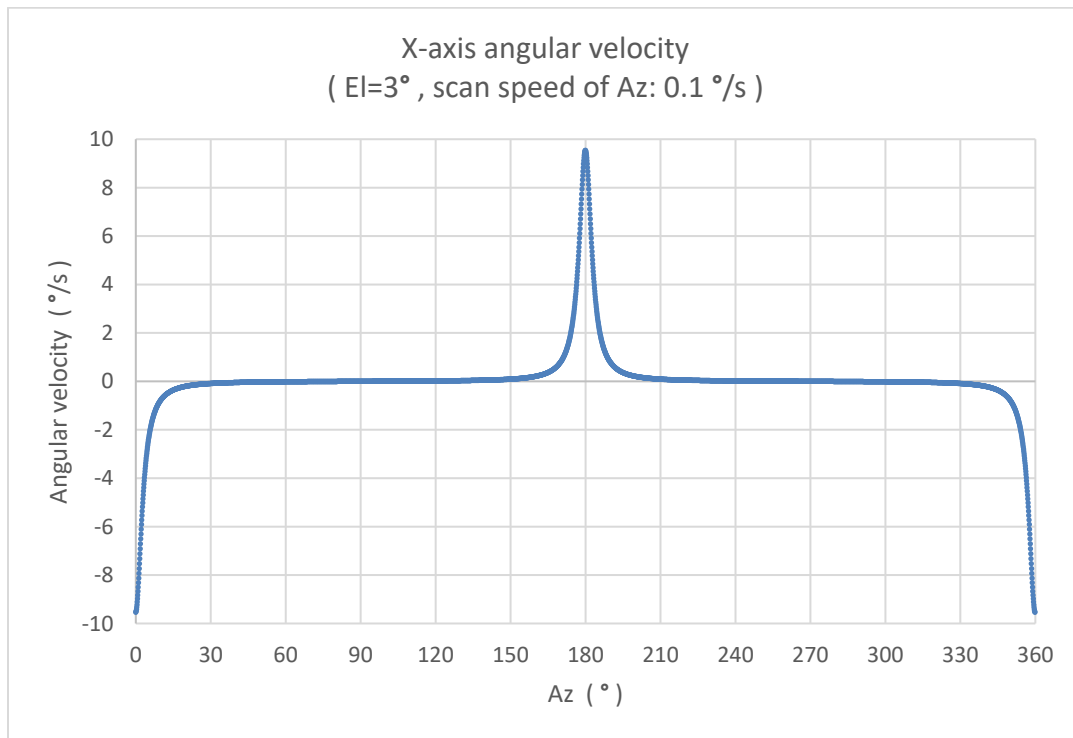


**Figure 2.5 The simulation of the X-axis rotation speed while scanning azimuth angles at the low elevation angle region (  $El = 3^\circ$  )**

As shown in Figure 2.5, the maximum value of the X-axis rotation speed in the simulation reaches  $9.54^\circ/\text{s}$ , far exceeding the maximum X-axis rotation speed ( $0.35^\circ/\text{s}$ )

that is limited specified for a physical system operating in satellite tracking mode.

In order to ensure the effective use of the antenna and the accuracy of the data, it is necessary to omit passes across the blind area of the antenna when setting up the satellite tracking schedule. According to Figure 2.6, the signal is of higher quality when the satellite reaches the zenith region above the ground station since there is a closer distance between the satellite and the ground station. As a result, most ground stations prefer the X-Y type antenna with a blind area in a low elevation area to the Az-El type antenna with a blind area in a zenith area.

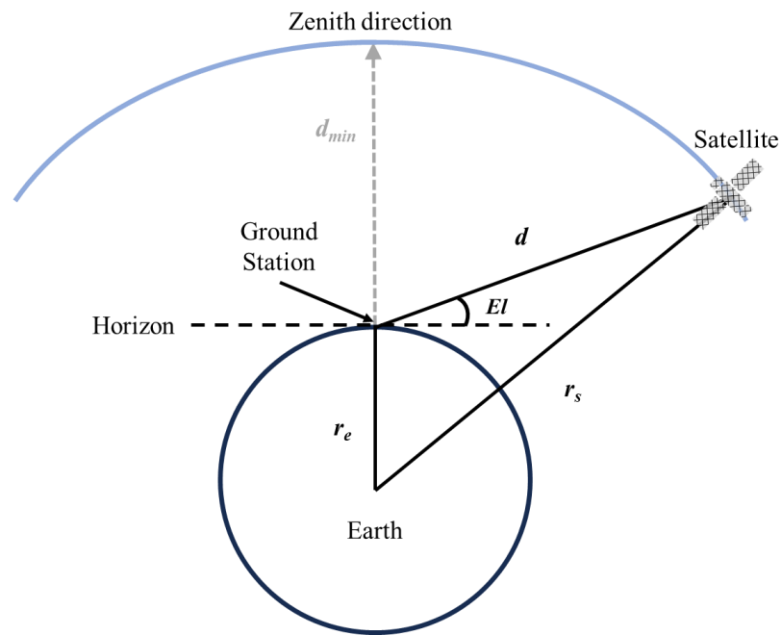


**Figure 2.6 The distance between the satellite and the ground station**

As depicted in Figure 2.6, we usually use azimuth-elevation angles when describing the geographical position of a satellite. However, to point the X-Y antenna in a specific direction, it is required to understand the angle at which the X- and Y-axes rotate. Therefore, the conversion of the X-Y angle to the Az-El angle is required. Figure 2.7

shows the relationship between the X-Y angle and the Az-El angle.

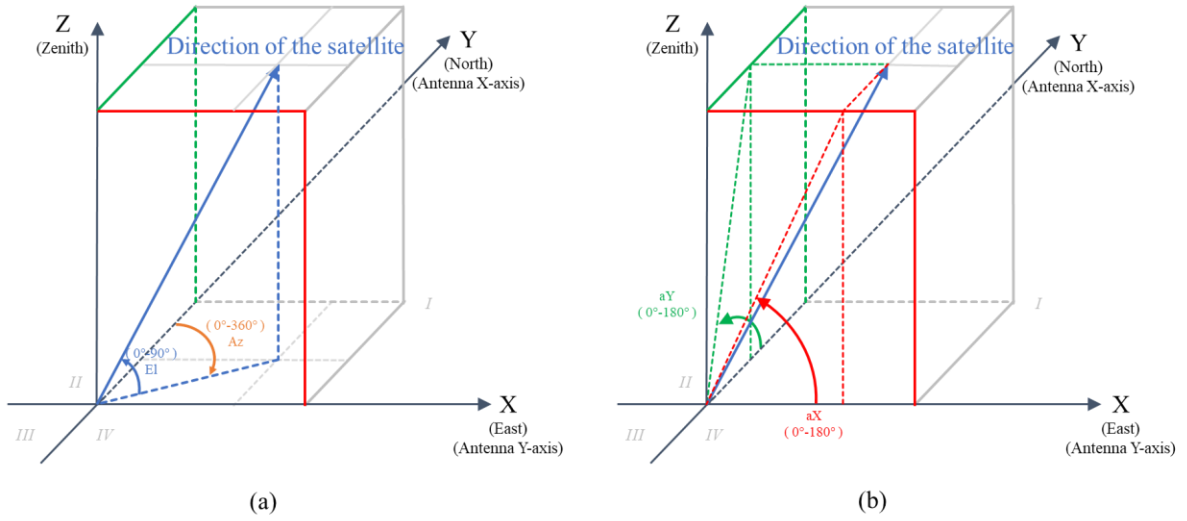


**Figure 2.7 The relationship between the Az-El angle and the X-Y angle:**  
**(a) Az-El angle (b) X-Y angle**

As shown in Figure 2.7, the X-axis of the antenna coincides with the direction of north, and the Y-axis of the antenna coincides with the direction of east. In Figure 2.7 (b),  $aX$  is the rotational angle of the X-axis, and  $aY$  is the rotational angle of the Y-axis. When calculating the X-Y angle according to the Az-El angle, a space rectangular coordinate system is established, like in Figure 2.7, to assist in the calculation. More specifically, let a vector of unit length in the direction of the satellite, then calculate the vector at coordinates  $(pX, pY, pZ)$  by Az-El angle as in Formula 2.1-2.3.

$$pX = \sin(Az)\cos(El) \quad (2.1)$$

$$pY = \cos(Az)\cos(El) \quad (2.2)$$

$$pZ = \sin(El) \quad (2.3)$$

After obtaining the coordinates of the unit vector  $(pX, pY, pZ)$ , according to the geometric relationship in Figure 2.7 (b), the rotation angle of the X-axis ( $aX$ ) and Y-axis

(aY) can be calculated as in Formula 2.4-2.5.

$$aX = \begin{cases} \arctan(pZ / pX), & pX > 0 \\ \arctan(pZ / pX) + 180^\circ, & pX < 0 \end{cases} \quad (2.4)$$

$$aY = \arccos\left(\frac{pY}{\sqrt{pY^2 + pZ^2}}\right) \quad (2.5)$$

## 2.2 Software systems

### 2.2.1 Overview

The highly automated satellite communication system (currently only reception ) at Kashiwa ground station was constructed by Astrocub Inc.. The system consists of three primary parts: Antenna control subsystem (built on antenna PC), Tracking receiver subsystem (built on TRRX PC), and Digital demodulator subsystem (built on HDRM PC). Figure 2.8 shows the hardware controlled by the corresponding subsystem.

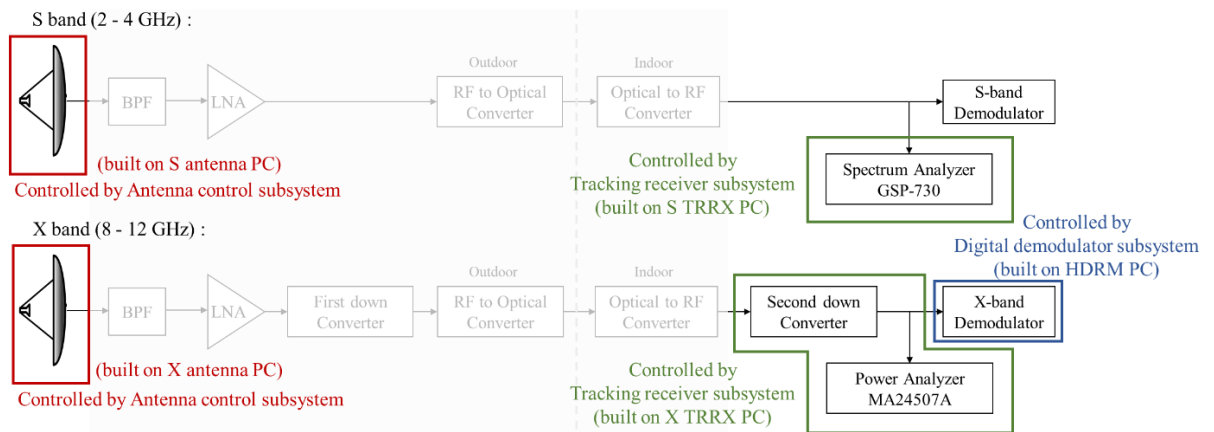


**Figure 2.8 The hardware controlled by the corresponding subsystem**

Figure 2.9 describes the interaction between the three subsystems. At the start and end

of the satellite signal reception, the antenna control subsystem will transmit specific messages from the antenna PC to the other PC over the network to start and stop the functioning of the other subsystems. The specifics will be presented in subsequent sections.

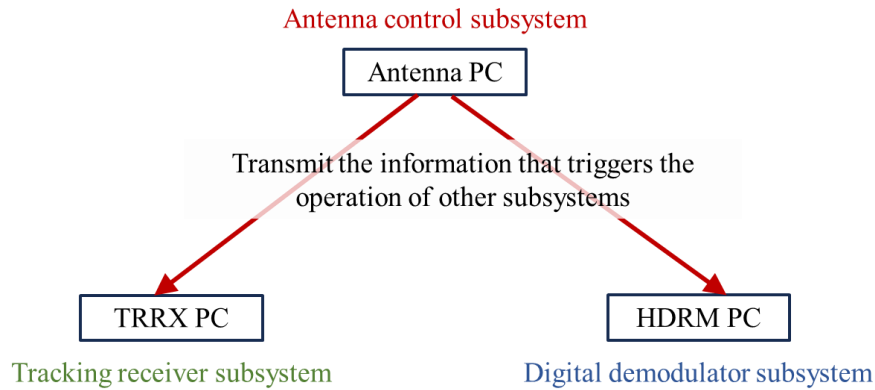


**Figure 2.9 The interaction between the three subsystems**

All PCs in the system are connected to the same local area network by a YAMAHA RTX1210 VPN router so that they can all be accessed and managed remotely through the remote desktop connection.

### **2.2.2 Antenna control subsystem**

The antenna control subsystem is the core part of the entire system and is responsible for driving the antenna and managing other subsystems. The system is built on the antenna PC, which is positioned next to the antenna on the roof of the experimental building (Figure 2.10).

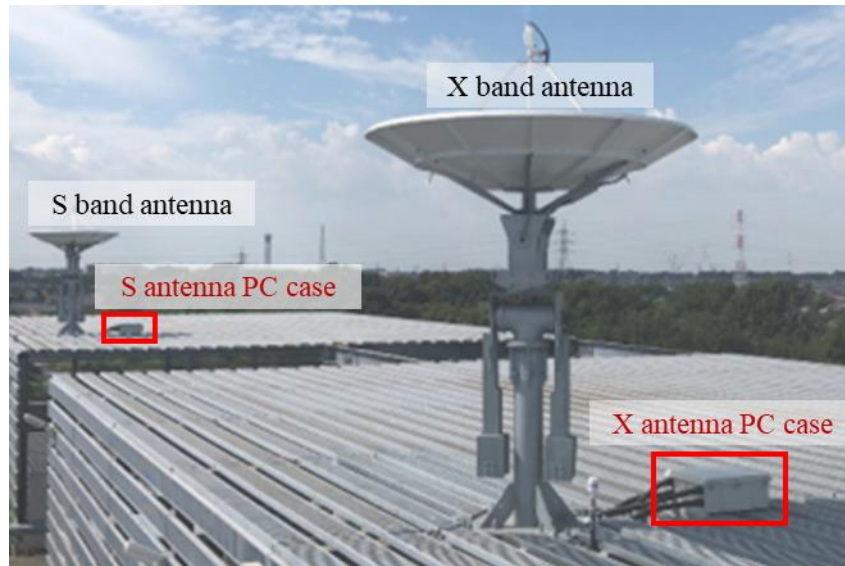


**Figure 2.10 The location of the antenna PC**

An antenna must be instructed on which direction to point when tracking a satellite. As a result, a satellite schedule (written in a Txt file) will contain information on the satellite's time-direction information as it passes the ground station. The file path, file name format, and content format of the schedule that the system can recognize are as follows:

**< SatelliteScheduleFile >**

**File path:** C:\AstroCub\schedule\

**File name format:** <SatelliteNORADNumber>\_<ScheduleStartTime>\_tr.txt

\* Example: 25994\_202307080112\_tr.txt

\* The schedule name of TERRA(25994) on 2023/07/08 starts at 01:12(UTC).

**File content format:**

<Date>	<Time>	<Az>	<El>	<Az>	<El>	<aX>	<aY>	<Distance>
2023/07/08	01:12:25.000	8.70640	3.03870	8.70640	3.03870	19.32550	9.21759	2758.717337
2023/07/08	01:12:25.200	8.70420	3.05240	8.70420	3.05240	19.41079	9.22000	2757.355420
2023/07/08	01:12:25.400	8.70200	3.06620	8.70200	3.06620	19.49662	9.22247	2755.993526
2023/07/08	01:12:25.600	8.69980	3.07990	8.69980	3.07990	19.58181	9.22493	2754.631653
2023/07/08	01:12:25.800	8.69760	3.09360	8.69760	3.09360	19.66696	9.22740	2753.269803
.....								

The schedule file's content is the satellite's direction relative to the ground station over

time. The Az-El angle and the calculation of the satellite-ground station distance will be introduced in 2.3.1. The aX-aY are the angles of rotation corresponding to the X-axis and Y-axis of the X-Y antenna, which is derived from the Az-El angle (introduced in chapter 2.1.2). The schedule should start from a full second (ss.000) and with a 0.2s time interval between rows. It should be mentioned that the satellite schedule should choose time intervals with the El angle greater than  $3^\circ$  during the satellite tracking to prevent antenna driving mistakes.

Secondly, the system also has an automatic schedule sorting function, which requires all the schedules of different satellites to be listed in a Txt file. The file path, file name, and content format are as follows:

**< ScheduleListFile >**

**File path:** C:\AstroCub\schedule\

**File name:** AntennaSchedule.txt

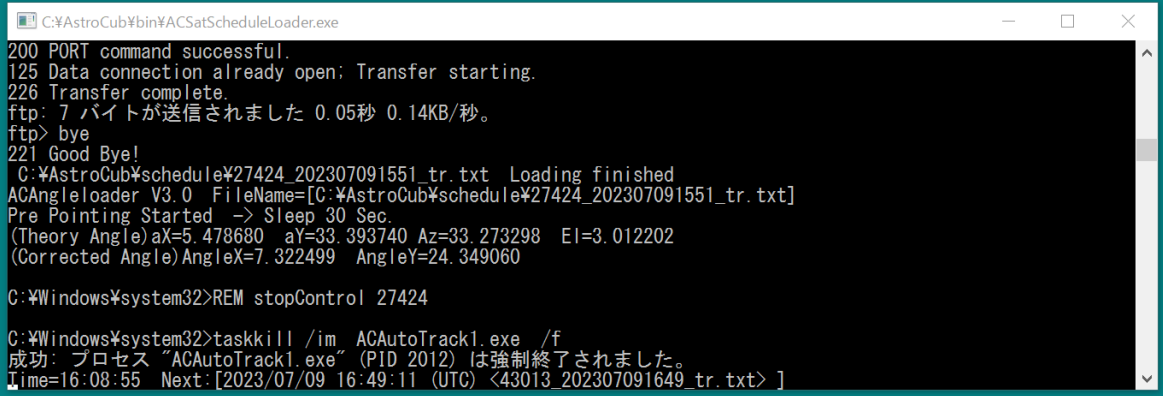
**Content format:**

<Satellite>	<Date>	<Start time>	<Date>	<Stop time>	<Max El>
25994	2023 07 08	01 12 25.0	2023 07 08	01 25 31.0	70.299
25994	2023 07 09	00 15 46.0	2023 07 09	00 28 01.0	27.437
27424	2023 07 08	03 08 50.0	2023 07 08	03 20 46.0	24.933
37849	2023 07 08	16 18 08.0	2023 07 08	16 32 48.0	77.736
37849	2023 07 10	03 19 34.0	2023 07 10	03 34 07.0	65.205
.....					

The start time is the time at which satellite tracking begins (the time found in the first line of the schedule file), and the stop time is the moment at which the antenna's drive comes to an end. In order to give the antenna enough time to return to its original position (point to the zenith) and lock the antenna to cease driving, the stop time should be set to a full second (ss.0) and around one minute after the end of satellite tracking (the time found in the last line of the schedule file). It is free to add new satellite schedules or remove existing ones at any time, and the system will scan this file at any

time to schedule the next antenna action time.

The primary software of the subsystem is ACSatScheduleLoader.exe. Figure 2.11 shows a screenshot of ACSatScheduleLoader.exe, with the progress of during satellite tracking showing on a window.



```
C:\AstroCub\bin\ACSatScheduleLoader.exe
200 PORT command successful.
125 Data connection already open; Transfer starting.
226 Transfer complete.
ftp: 7 バイトが送信されました 0.05秒 0.14KB/秒。
ftp> bye
221 Good Bye!
C:\AstroCub\schedule\27424_202307091551_tr.txt Loading finished
ACAngleloader V3.0 FileName=[C:\AstroCub\schedule\27424_202307091551_tr.txt]
Pre Pointing Started -> Sleep 30 Sec.
(Theory Angle) aX=5.478680 aY=33.393740 Az=33.273298 El=3.012202
(Corrected Angle) AngleX=7.322499 AngleY=24.349060

C:\Windows\system32>REM stopControl 27424

C:\Windows\system32>taskkill /im ACAutoTrack1.exe /f
成功: プロセス "ACAutoTrack1.exe" (PID 2012) は強制終了されました。
Time=16:08:55 Next:[2023/07/09 16:49:11 (UTC) <43013_202307091649_tr.txt> ]
```

**Figure 2.11 The window of ACSatScheduleLoader.exe**

ACSatScheduleLoader.exe is responsible for driving the antenna according to the schedule, controlling other subsystems, and starting the antenna drive logging module.

Figure 2.12 depicts the functional flowchart of ACSatScheduleLoader.exe.

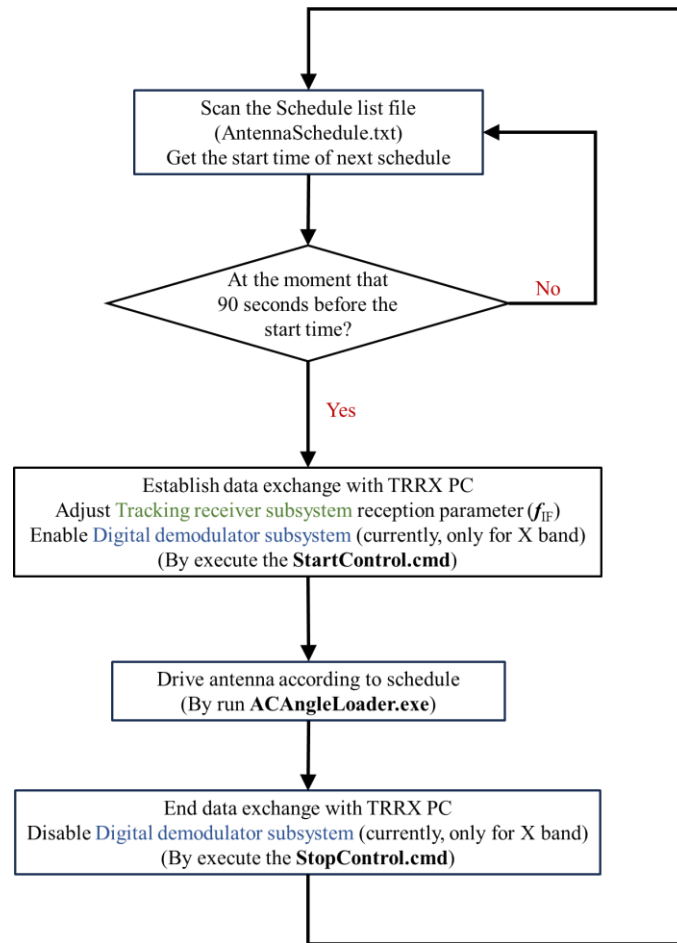


**Figure 2.12 The functional flowchart of ACSatScheduleLoader.exe**

ACSatScheduleLoader.exe consists of three essential components: StartControl.cmd, ACAngleLoader.exe, and StopControl.cmd. The details are described as follows:

- **<StartControl.cmd>**

**File path:** C:\AstroCub\control\

**File name format:** StartControl\_<SatelliteNORADNumber>.cmd

\* Example: StartControl\_25994.cmd

**File content (StartControl\_25994.cmd as an example):**

```

c:\AstroCub\bin\AcPolarityControl.exe RHCP
copy C:\AstroCub\param\satellite\Satellite_25994.txt C:\AstroCub\param\satellite\SatelliteName.txt
start c:\AstroCub\bin\ACAutoTrack1.exe
ftp -n -s:C:\AstroCub\param\tuner\tuner25994.ftp
  
```

ftp -n -s:C:\AstroCub\param\hdrm\hdrm25994.ftp

**Explanation:**

Line 1: Select the polarization mode for the satellite that was received. (RHCP / LHCP)

Line 2: Upload the satellite name that matches the satellite NORAD number.

The Txt file with the satellite name in the content must be named using the prescribed format and be located in the specified path:

ex: C:\AstroCub\param\satellite\Satellite\_25994.txt

Line 3: Run ACAutoTrack1.exe.

ACAutoTrack1.exe performs two functions:

- (1) Establish socket connection with TRRX PC and read the measurement value of the received signal intensity from the measuring instrument (Spectrum Analyzer/Power Analyzer).
- (2) Correcting the pointing orientation of satellite in real-time for alignment (the specific theory is described in chapter 2.3.2).

Line 4: Execute the tuner Ftp file to transfer the Txt file with the  $f_{IF}$  parameter of the Tracking receiver subsystem to the TRRX PC.

Some more detailed explanations are as follows :

- (1) For the S band,  $f_{IF}$  is the center frequency of the received signal and is used to modify the center frequency that the Spectrum Analyzer is watching.
- (2) For the X band,  $f_{IF}$  can be calculated as in Formula 2.6.

$$f_{IF} = f_{\text{Satellite signal}} - 6000 - 720 \quad (2.6)$$

The unit in Formula 2.6 is MHz.  $f_{IF}$  represents the frequency that needs to be downconverted at the second downconverter. (Attend that the demodulator (HDRM) required a 720MHz signal, and the first downconverter allowed the

received signal frequency to be downconverted 6000MHz. )

(3) Note the Ftp file and the Txt file with the  $f_{IF}$  parameter in the content must be named using the prescribed format and be located in the specified path:

ex: C:\AstroCub\param\tuner\tuner25994.ftp

C:\AstroCub\param\tuner\tuner25994.txt

Line 5: Execute the hdrm Ftp file to transfer the Txt file that can enable the digital demodulator subsystem to the HDRM PC. (Currently, only for X band)

Note the Ftp file and the Txt file with the satellite NORAD number in the content must be named using the prescribed format and be located in the specified path:

ex: C:\AstroCub\param\hdrm\hdrm25994.ftp

C:\AstroCub\param\hdrm\hdrm25994.txt

#### • **ACAngleLoader.exe**

ACAngleLoader.exe is responsible for driving the antenna according to the schedule and starting the antenna drive logging module. Before introducing the functions implemented by ACAngleLoader.exe, it is necessary to comprehend how the antenna control subsystem enables data sharing between multiple software.

Most of the software for the antenna control subsystem is developed in C. In 32-bit windows, the physical memory can be mapped to a file using the CreateFileMapping() function and MapViewOfFile() function to quickly share the memory by accessing the file for reading and writing. The antenna control subsystem has two main shared files, named "MotorStateServer" and "AngleDataServer", which are described as follows:

#### **"MotorStateServer"**

Type: Integer array

[0] Control the stopping or moving mode of the motor.

- value: 0    Stop Mode
- 1    Satellite Servo Mode (Low-speed moving mode)
- 2    Pointing Mode (High-speed moving mode)

[1] The Flag that controls the recording module.

- value: 0    Stop Recording
- 1    Start Recording

## **"AngleDataServer"**

Type: Double array

The parameter for the antenna pointing drive.

[0] Angle of Axis-X with physical alignment model [degree] ( calculate by [8] )

[1] Angle of Axis-Y with physical alignment model [degree] ( calculate by [9] )

[8] Target Angle of Axis-X [degree] ( upload by schedule file )

[9] Target Angle of Axis-Y [degree] ( upload by schedule file )

[10] error of Axis-X [degree] ( = [0]-[8] )

[11] error of Axis-Y [degree] ( = [1]-[9] )

[12] Auto offset of Axis-X [degree] ( upload by ACAutoTrack1.exe)

[13] Auto offset of Axis-Y [degree] ( upload by ACAutoTrack1.exe)

[14] Az [degree] ( convert by [0], [1] )

[15] El [degree] ( convert by [0], [1] )

[19] Angle Error in Az [degree] ( convert by [10], [11] )

[20] Angle Error in El [degree] ( convert by [10], [11] )

[24] Intensity of the received signal ( upload by ACAutoTrack1.exe)

[25] Distance between satellite and ground station [km] ( upload by schedule file )

[104] Az offset Factor [degree] ( upload by C:\AstroCub\param\antenna\Az.txt)

The system will continue to read the value of "MotorStateServer" to start or stop the motor and the value of "AngleDataServer" ([8], [9], [12], [13]) to set the antenna's pointing direction. Therefore, ACAngleLoader.exe is responsible for continuously writing to "MotorStateServer" and "AngleDataServer" to drive the antenna and control the recording module. Figure 2.13 depicts the functional flowchart of ACAngleLoader.exe.

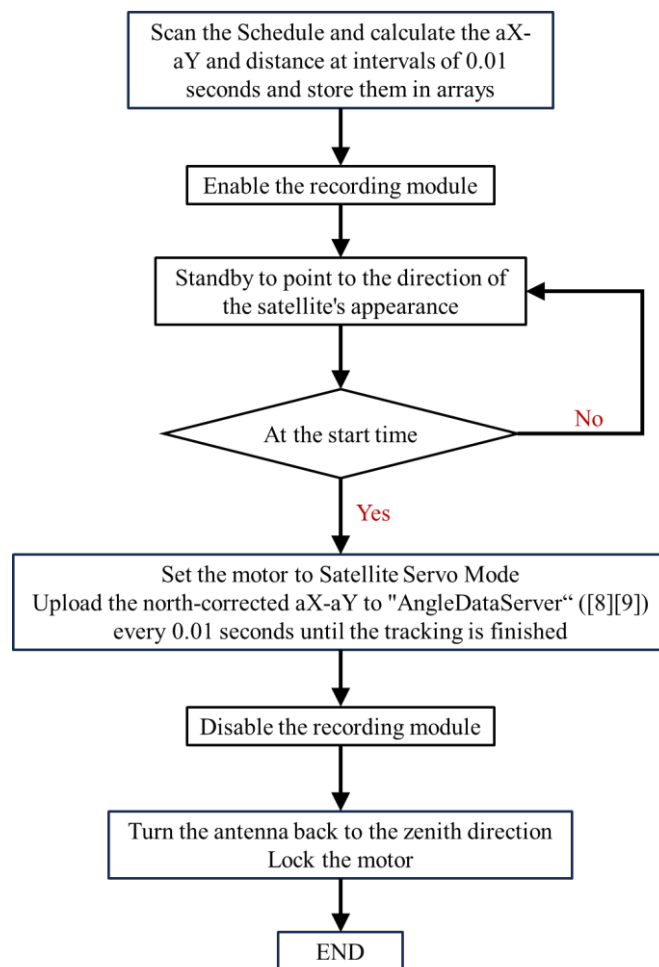


**Figure 2.13 The functional flowchart of ACAngleLoader.exe**

The recording module consists of ACServoRecorder.exe and ACAnglerecorder.exe.

Figure 2.14 shows the screenshots of the windows of both software.

**Figure 2.14 The window of the recording module**

ACServoRecorder.exe records data from "MotorStateServer" and "AngleDataServer" during satellite tracking and saves it to a Txt file (path: C:\AstroCub\logs\Servo\). ACAnglerecorder.exe records data only from "AngleDataServer" and saves it to a Txt file (path: C:\AstroCub\logs\Angle\). The file record by ACAnglerecorder.exe serves typically to determine whether the satellite signal was successfully received, and its contents are as follows:

```
<Date>      <Time>      [0]      [1]      [8]      [9]      [10]     [11]     [12]     [13]     [14]     [15]     [19]     [20]     [25]     [24]     [26]     [27]
2023/03/27 12:21:33.15 89.9734 89.8138 90.0000 90.0000 -0.0266 -0.1862 0.0000 0.0000 8.1289 89.8119 359.8138 0.0001 -21.471954 0.000000 0.000000 0.000000
2023/03/27 12:21:33.35 89.9734 89.8138 90.0000 90.0000 -0.0266 -0.1862 0.0000 0.0000 8.1289 89.8119 359.8138 0.0001 -21.471954 0.000000 0.000000 0.000000
2023/03/27 12:21:33.55 89.9734 89.8138 90.0000 90.0000 -0.0266 -0.1862 0.0000 0.0000 8.1289 89.8119 359.8138 0.0001 -21.471954 0.000000 0.000000 0.000000
.....
```

• **<StopControl.cmd>**

**File path:** C:\AstroCub\control\

**File name format:** StopControl\_<SatelliteNORADNumber>.cmd

\* Example: StopControl\_25994.cmd

**File content (StopControl\_25994.cmd as an example):**

```
REM stopControl 25994
taskkill /im ACAutoTrack1.exe /f
ftp -n -s:C:\AstroCub\param\hdrm\hdrm00000.ftp
```

### Explanation:

Line 1: Just a note of satellite NORAD number.

Line 2: Stop the ACAutoTrack1.exe from running.

Close the socket connection to the TRRX PC.

Line 3: Execute the hdrm Ftp file to transfer the Txt file that can disable the digital demodulator subsystem to the HDRM PC. (Currently, only for X band)

Note the Ftp file and the Txt file with '00000' in the content must be named using the prescribed format and be located in the specified path:

C:\AstroCub\param\hdrm\hdrm00000.ftp

C:\AstroCub\param\hdrm\hdrm00000.txt

In addition, in this subsystem, SetAngleXY4.exe supports positioning the antenna in a specified direction. Figure 2.15 shows the window of SetAngleXY4.exe.

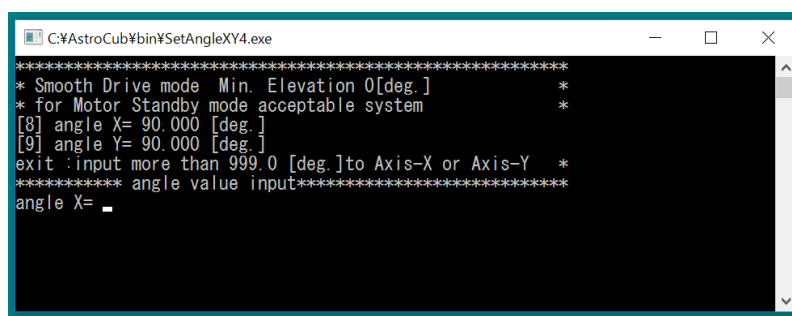


**Figure 2.15 The window of SetAngleXY4.exe**

While pointing in a specified direction, enter the Az-El angle of the direction that was transformed to an aX-aY angle after taking into account the north correction(introduced in Chapter 3.1) into the software. If the input value exceeds 999, the antenna motor will

be locked. It should be noted that after use, the antenna must be rotated back to the zenith direction ( $aX=90^\circ$ ,  $aY=90^\circ$ ) and lock the motor.

The subsystem also features a monitor module comprising readangle2.exe and ACECmonitor.exe to more intuitively know the current antenna pointing direction and motor status. Figure 2.16 shows the screenshots of the windows of both software.

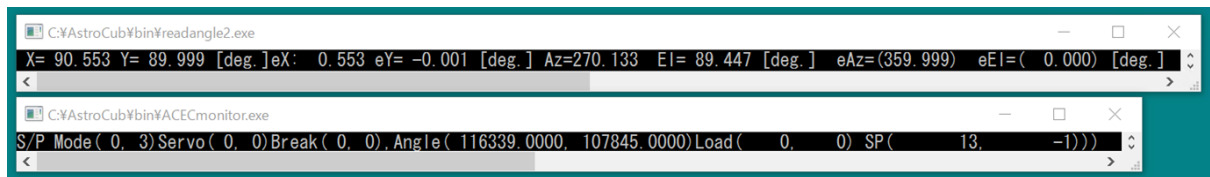


**Figure 2.16 The window of the monitor module**

readangle2.exe shows the antenna pointing information from "AngleDataServer". ACECmonitor.exe shows the motor's state. The details of ACECmonitor.exe are as follows:

Servo, Break: Motor status

Servo(0,0) Break(0,0): Locked

Servo(1,1) Break(1,1): Unlocked

Angle: Accumulated rotation angle of the X-axis and Y-axis

SP: Rotation speed of the motor

### 2.2.3 Tracking receiver subsystem

The tracking receiver subsystem is mainly responsible for establishing the socket connection between TRRX PC and antenna PC for data transfer and controlling the spectrum analyzer(S band) or downconverter(X band). The tracking receiver subsystem

is built on the TRRX PC, and figure 2.17 shows the physical layout of the TRRX PC.

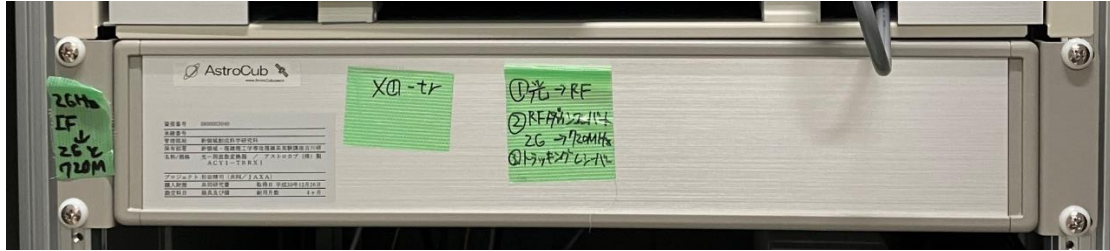


**Figure 2.17 The physical layout of the TRRX PC**

TRRXControlRequest.exe is the primary software used for hardware control. Figure 2.18 shows the screenshot of the TRRXControlRequest.exe window.

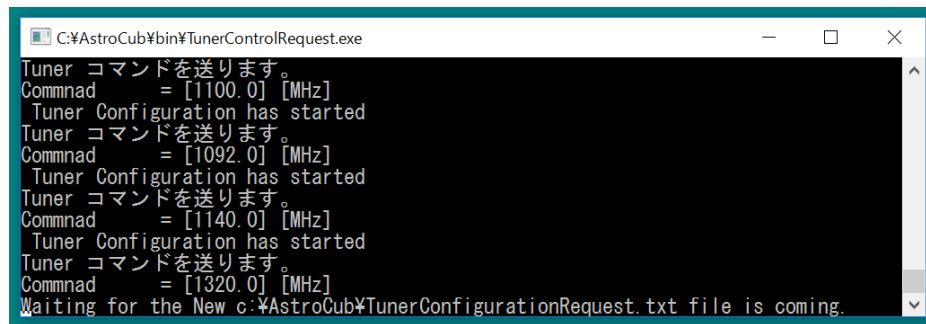


**Figure 2.18 The window of TRRXControlRequest.exe**

Before tracking the satellite, the antenna PC will send a Txt file named TunerConfigurationRequest.txt to the TRRX PC (path: C:\AstroCub\ ) with the  $f_{IF}$  parameter written in the file (as explained in Chapter 2.2.2). TRRXControlRequest.exe will keep checking whether the TunerConfigurationRequest.txt file exists. If the file is present, TRRXControlRequest.exe will adjust the hardware parameters according to the  $f_{IF}$  parameter in the file. Figure 2.19 depicts the functional flowchart of TRRXControlRequest.exe.

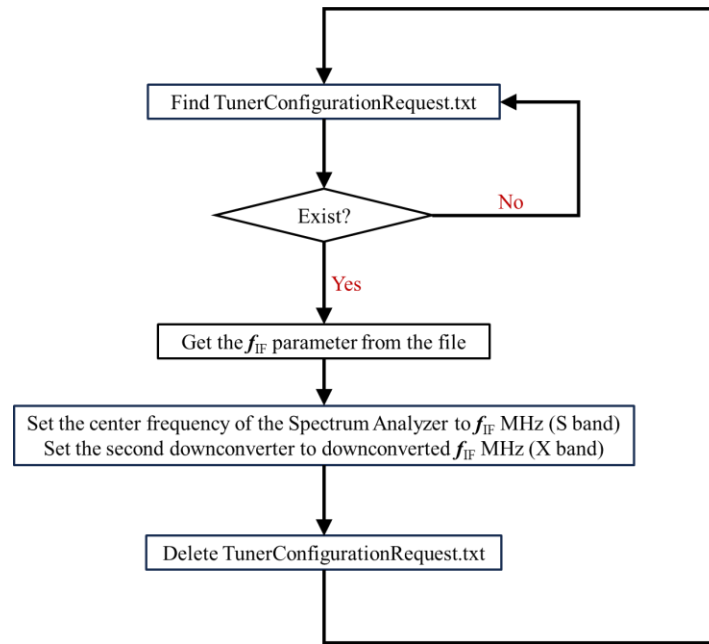


**Figure 2.19 The functional flowchart of TRRXControlRequest.exe**

As shown in Figure 2.19, the file will be deleted after each setup to guarantee that parameter adjustments to the hardware are made only once before each satellite tracking.

Another essential part is the measurement module, which reads the intensity of the received signal measured by the measurement instrument and displays the value in the window (as shown in Figure 2.20). More importantly, this module is responsible for uploading the measurement data to the shared memory (S: "SPECTRUM\_POWER" X: "POWER\_DATA").

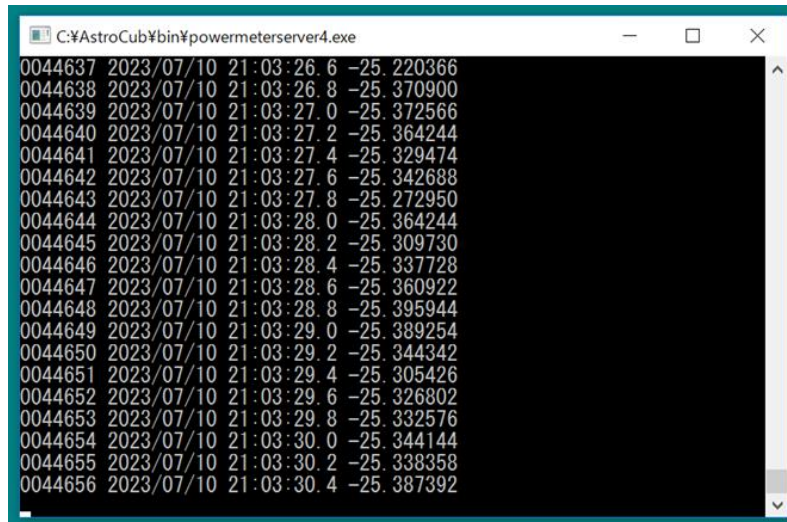


**Figure 2.20 The window of Measurement module**

Additionally, AutoTrackPortPort.exe is used to establish a socket connection to exchange data with the antenna PC. It transfers the signal strength data from the TRRX PC's shared memory to the antenna PC. Figure 2.21 shows the screenshot of the AutoTrackPort.exe window.

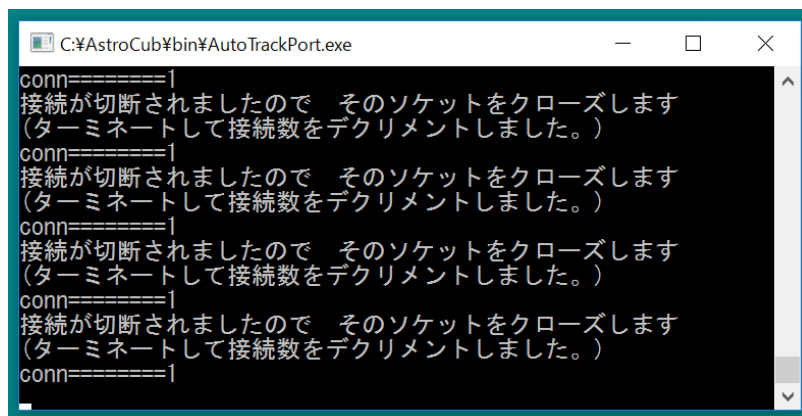


**Figure 2.21 The window of AutoTrackPort.exe**

When other PCs establish the socket connection with TRRX PC (such as when antenna pc runs ACAutoTrack1.exe), the number of connections will be displayed in the window. The window will also show that the connection has been closed when others

shut the socket connection(such as when the antenna PC terminated ACAutoTrack1.exe).

## 2.2.4 Digital demodulator subsystem

The Digital demodulator subsystem is responsible for the automatic demodulation function during satellite tracking. The demodulator used in the Kashiwa ground Station is the High Data Rate Modem (HDRM), which has an integrated PC. Figure 2.17 shows the physical layout of the HDRM.



**Figure 2.22 The physical layout of the HDRM**

HDRMControlServer.exe is the leading software of the Digital demodulator subsystem, which has almost the same function as the TRRXControlRequest.exe described in Chapter 2.2.3. It waits for the antenna PC to send a file containing information about the NORAD number of the satellite or 00000(stop flag), to start or stop the related demodulation automatically. Figure 2.23 shows the screenshot of this software window.

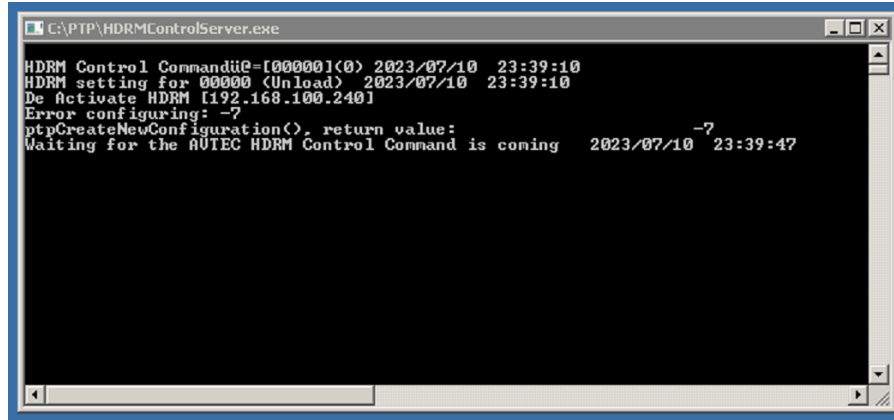


Figure 2.23 The window of HDRMControlServer.exe

## 2.3 Satellite tracking technology

### 2.3.1 Satellite position calculation

The Kashiwa ground station receives Earth observation satellites flying in low-Earth orbit (LEO) with 250–2000 km altitudes. This Chapter will show a quick and simple method for forecasting an LEO satellite's future position. The calculation will use the TLE data published by NORAD on the web (<https://celestrak.org/NORAD/elements/>) and only consider the perturbations brought on by the earth's oblateness.

The position and motion of a LEO satellite in ECI coordinate system can be described by orbital elements as in Formula 2.7.

$$X = (a, e, i, \Omega, \omega, \theta) \quad (2.7)$$

The physical significance of orbital elements is shown in Figure 2.24.

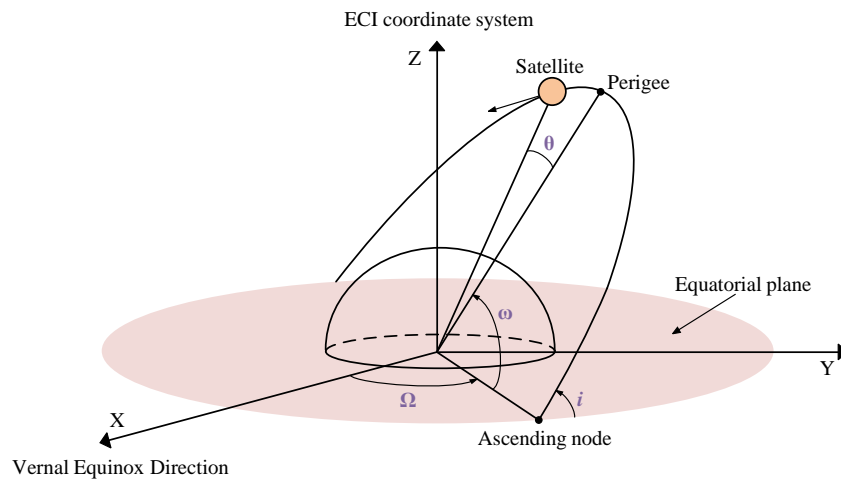


**Figure 2.24 The physical significance of orbital elements (ECI)**

More detailed definitions are as follows:

The elements define the shape and size of the ellipse:

- **a** semimajor axis
- **e** eccentricity

The elements define the orientation of the orbital plane:

- **i** inclination
- **Ω** longitude of the ascending node

The elements define the orientation of the ellipse in the orbital plane:

- **ω** argument of perigee

The elements define the position of the orbiting body along the ellipse:

- **θ** true anomaly

The satellite position forecast is calculated by a specific perturbation model that uses the satellite position (orbit elements) at a given moment as input. The calculation takes TLE data as input, and the perturbation model solely considers the effects of the earth's oblateness. Therefore, only the variation of **a**, **Ω**, **ω**, and **θ** with time is calculated, and

the variation of  $\mathbf{e}$  and  $\mathbf{i}$  with time is neglected (as in Formula 2.8).

$$\left[ t = t_0, X_0 = (a_0, e_0, i_0, \Omega_0, \omega_0, \theta_0) \right] \rightarrow \left[ t = t_k, X_{t_k} = (a_{t_k}, e_0, i_0, \Omega_{t_k}, \omega_{t_k}, \theta_{t_k}) \right] \quad (2.8)$$

Some of the orbital elements in Formula 2.7 do not come out directly in the TLE data. Therefore, some of the orbital elements at the target moment are not calculated, but other elements equivalence to those are calculated. In addition, to know the pointing direction of the antenna during satellite tracking, the ultimate goal of satellite position forecast is to obtain the satellite's position in the topocentric coordinate system. From this, the Az-El angle used for antenna driving and the distance between the satellite and the ground station can be calculated. The specific calculation method is as follows:

### 1. The content of the TLE data

TLE :

DMSP 5D-3 F17 (USA 191)	$t_0$	$M_2$				
1 29522U 06050A	<u>22359.82342486</u>	<u>.000000099</u>	00000+0	74672-4	0	9996
2 29522	<u>98.7605</u>	<u>11.2383</u>	<u>0010808</u>	<u>78.1499</u>	<u>282.0886</u>	<u>14.14151956</u> 332958
	$i_0$	$\Omega_0$	$e_0$	$\omega_0$	$M_0$	$M_1 (a_0)$

**Figure 2.25 An example of the TLE data**

Figure 2.25 labels the variables that will be utilized in the calculation. The detailed explanations from the first row are as follows:

- (1)  $t_0 = 359.82342486$  (day) // Epoch Time  
// The time that had elapsed in 2022 when this TLE data were determined.
- (2)  $M_2 = 0.000000099$  (rev/day<sup>2</sup>) // First Time Derivative of Mean Motion
- (3)  $i_0 = 98.7605$  (degree) // Inclination
- (4)  $\Omega_0 = 11.2383$  (degree) // Longitude of the ascending node
- (5)  $e_0 = 0.0010808$  // Eccentricity
- (6)  $\omega_0 = 78.1499$  (degree) // Argument of perigee

(7)  $M_0 = 282.0886$  (degree) // Mean Anomaly

(8)  $M_1 = 14.14151956$  (rev/day) // Mean Motion (Mean orbital period)

//  $a_0$  can be calculated by Kepler's third law with  $M_1$ .

## 2. Calculation of $a_{tk}$

The mean motion (mean orbital period) at the time  $t_k$  is calculated as in Formula 2.9.

$$M_m = M_1 + M_2 (t_k - t_0) \quad (2.9)$$

The orbital semimajor axis at the time  $t_k$  can be calculated by Kepler's third law as in Formula 2.10.

$$a_{t_k} = \left( \frac{GM}{4\pi^2 M_m^2} \right)^{\frac{1}{3}} \quad (2.10)$$

Where  $GM = 2.975537 \times 10^{15} (\text{km}^3/\text{day}^2)$  is the standard gravitational parameter of the Earth.

## 3. Calculation of satellite position in perifocal coordinate system (equivalent to $\theta_{tk}$ )

This part calculates the satellite's position along the ellipse ( $\theta$  in the orbit element) at time  $t_k$ . This physical quantity is typically expressed using the satellite's coordinates (U,V) in the perifocal coordinate system to make subsequent computations easier. The perifocal coordinate system has the Earth as its origin, and the specific geometric relationship is shown in Figure 2.26.

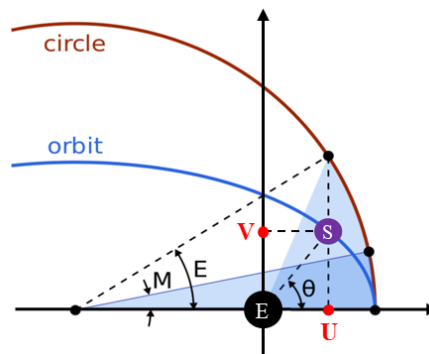


Figure 2.26 Satellite's position in perifocal coordinate system

The geometric relationship between the eccentric anomaly (E) and the true anomaly ( $\theta$ ) is shown in Figure 2.26. Based on the geometric relationship in the figure, the coordinates (U,V) are calculated as in Formula 2.11-2.12.

$$U_{t_k} = a_{t_k} \cos E_{t_k} - a_{t_k} e_0 \quad (2.11)$$

$$V_{t_k} = a_{t_k} \sqrt{1-e_0^2} \sin E_{t_k} \quad (2.12)$$

However, the TLE data are not provided information on eccentric anomaly (E), only provide information on mean anomaly (M). The mean anomaly is the fraction of an elliptical orbit's period that has elapsed since the orbiting body passed periapsis, expressed as an angle. It is the angular distance from the pericenter which a fictitious body would have if it moved in a circular orbit, with constant speed, in the same orbital period as the actual body in its elliptical orbit. The relationship between mean anomaly (M) and eccentric anomaly (E) is shown in Equation 2.13.

$$E_{t_k} - e_0 \sin E_{t_k} = M_{t_k} \quad (2.13)$$

Where the mean anomaly (M) at the time  $t_k$  can be calculated from the parameters given in TLE data as in Formula 2.14.

$$M_{t_k} = M_0 + M_1(t_k - t_0) + \frac{1}{2}M_2(t_k - t_0)^2 \quad (2.14)$$

Equation 2.13, also known as Kepler's equation. The eccentric anomaly (E) can be solved iteratively via the Newton-Raphson method.

#### 4. Calculation of $\Omega_{tk}$ and $\omega_{tk}$

Earth's oblateness would cause secular perturbations of  $\Omega$  and  $\omega$ . Secular perturbations cause orbital elements to increase or decrease unilaterally with time, and therefore the change in orbital elements with time is calculated by the average rate as in Formula 2.15-2.16.

$$\Omega_{t_k} = \Omega_0 + \dot{\Omega}_{\text{avg}} (t_k - t_0) \quad (2.15)$$

$$\omega_{t_k} = \omega_0 + \dot{\omega}_{\text{avg}} (t_k - t_0) \quad (2.16)$$

The expressions for the average rate of precession are shown in Formula 2.17-2.18.

$$\dot{\Omega}_{\text{avg}} = - \left[ \frac{3\sqrt{GM} J_2 R^2}{2(1-e_0^2)^2 a_{t_k}^{\frac{7}{2}}} \right] \cos i_0 \quad (2.17)$$

$$\dot{\omega}_{\text{avg}} = - \left[ \frac{3\sqrt{GM} J_2 R^2}{2(1-e_0^2)^2 a_{t_k}^{\frac{7}{2}}} \right] \left( \frac{5}{2} \sin^2 i_0 - 2 \right) \quad (2.18)$$

Where  $GM = 2.975537 \times 10^{15} (\text{km}^3/\text{day}^2)$  is the standard gravitational parameter of the Earth,  $J_2 = 0.00108263$  is the second zonal harmonic of the Earth,  $R = 6378.137$  (km) is the mean equatorial radius of the Earth. Note that the units for the  $\dot{\Omega}_{\text{avg}}$  and  $\dot{\omega}_{\text{avg}}$  in Formula 2.17-2.18 are (rad/day). Honestly, the strongest enemy in calculations is the conversion of units.

## 5. Calculation of satellite position in ECI coordinate system

The ECI coordinate system has its origin at the center of the Earth, an X-axis that points toward the vernal equinox, a Z-axis that points toward the North Pole, and a Y-axis that is positioned so that the three axes form a dextral coordinate system. Figure 2.27 shows the relationship in space between the perifocal coordinate system and the ECI coordinate system.

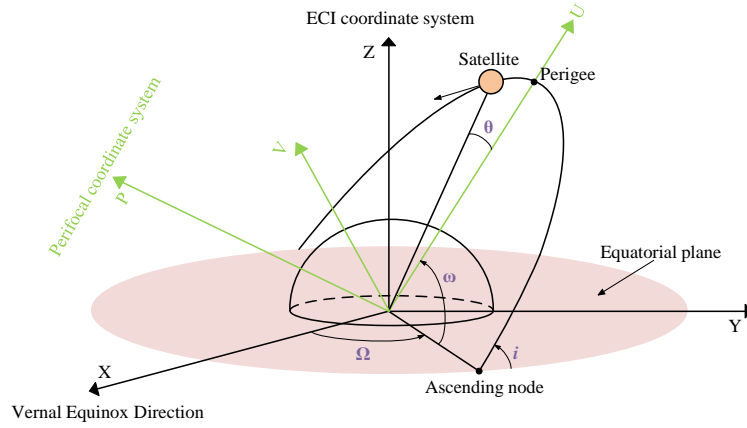


**Figure 2.27 The relationship in space between the perifocal coordinate system and the ECI coordinate system**

As shown in Figure, if the perifocal coordinate system is rotated in the following order:

Rotate the P-axis clockwise by  $\omega$  degrees.

Rotate the U-axis clockwise by  $i$  degrees.

Rotate the P-axis clockwise by  $\Omega$  degrees.

Then the perifocal coordinate system will coincide with the ECI coordinate system.

Therefore, the coordinates in the perifocal coordinate system  $(U, V, 0)^T$  can be multiplied by the above three rotation matrices to obtain the coordinates in the ECI coordinate system  $(X, Y, Z)^T$  (as shown in Formula 2.19).

$$\begin{pmatrix} X \\ Y \\ Z \end{pmatrix}_{ECI} = \begin{pmatrix} \cos \Omega_{t_k} & -\sin \Omega_{t_k} & 0 \\ \sin \Omega_{t_k} & \cos \Omega_{t_k} & 0 \\ 0 & 0 & 1 \end{pmatrix} \begin{pmatrix} 1 & 0 & 0 \\ 0 & \cos i_0 & -\sin i_0 \\ 0 & \sin i_0 & \cos i_0 \end{pmatrix} \begin{pmatrix} \cos \omega_{t_k} & -\sin \omega_{t_k} & 0 \\ \sin \omega_{t_k} & \cos \omega_{t_k} & 0 \\ 0 & 0 & 1 \end{pmatrix} \begin{pmatrix} U \\ V \\ 0 \end{pmatrix} \quad (2.19)$$

## 6. Calculation of satellite position in ECEF coordinate system

The ECEF coordinate system has its origin at the center of the Earth, an X-axis that points toward the Prime meridian, a Z-axis that points toward the North Pole, and a Y-axis that is positioned so that the three axes form a dextral coordinate system. Figure 2.28 shows the relationship in space between the ECI coordinate system and the ECEF coordinate system.

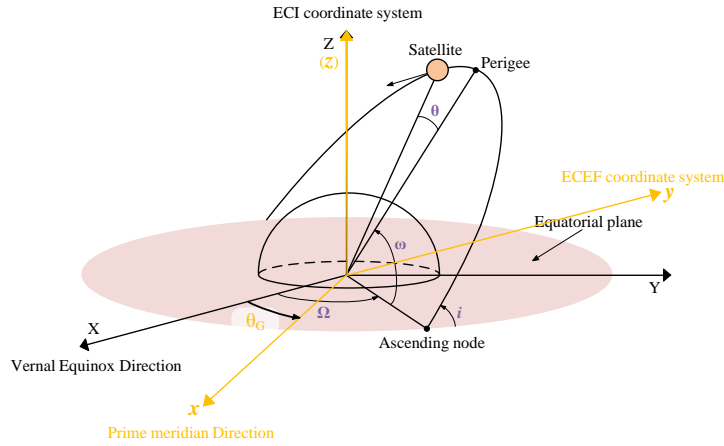


**Figure 2.28 The relationship in space between the ECI coordinate system and the ECEF coordinate system**

$\theta_G$  in the figure is the angle between the direction of the Prime meridian and the direction of the vernal equinox. ECI coordinate system is fixed with respect to the center of the Earth in contrast to the ECEF coordinate system, which remains fixed with respect to Earth's surface and rotates with the Earth. According to the geometric relationship in Figure 2.28, the coordinates in the ECEF coordinate system are calculated as shown in Formula 2.20.

$$\begin{pmatrix} x \\ y \\ z \end{pmatrix}_{ECEF} = \begin{pmatrix} \cos \theta_G & \sin \theta_G & 0 \\ -\sin \theta_G & \cos \theta_G & 0 \\ 0 & 0 & 1 \end{pmatrix} \begin{pmatrix} X \\ Y \\ Z \end{pmatrix}_{ECI} \quad (2.20)$$

## 7. Calculation of satellite position in topocentric coordinate system

The topocentric coordinate system has its origin at the center of the observation position (Kashiwa ground station), an X-axis that points to east, a Z-axis that points to zenith, and a Y-axis that points to north. Figure 2.29 shows the relationship in space between the ECEF coordinate system and the topocentric coordinate system.

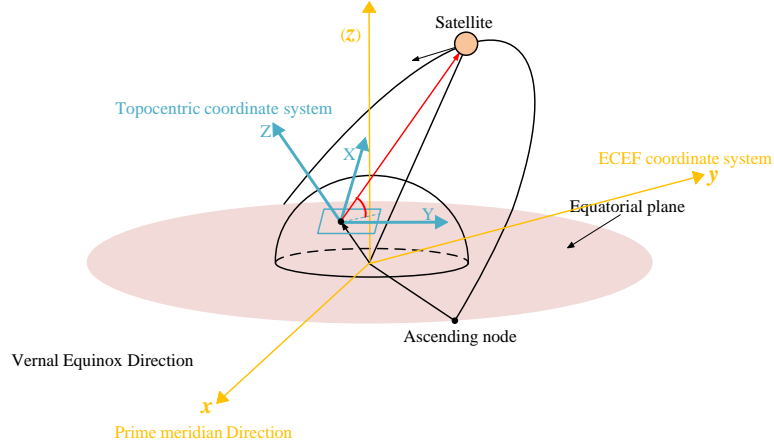


**Figure 2.29 The relationship in space between the ECEF coordinate system and the topocentric coordinate system**

The coordinates in the topocentric coordinate system are calculated as shown in Formula 2.21.

$$\begin{pmatrix} X \\ Y \\ Z \end{pmatrix}_{ENU} = \begin{pmatrix} \cos 90^\circ & \sin 90^\circ & 0 \\ -\sin 90^\circ & \cos 90^\circ & 0 \\ 0 & 0 & 1 \end{pmatrix} \begin{pmatrix} \cos(90^\circ - lat) & 0 & -\sin(90^\circ - lat) \\ 0 & 1 & 0 \\ \sin(90^\circ - lat) & 0 & \cos(90^\circ - lat) \end{pmatrix} \begin{pmatrix} \cos(lon) & \sin(lon) & 0 \\ -\sin(lon) & \cos(lon) & 0 \\ 0 & 0 & 1 \end{pmatrix} \begin{pmatrix} X \\ Y \\ Z \end{pmatrix}_{ECEF} - \begin{pmatrix} 0 \\ 0 \\ R_E \end{pmatrix} \quad (2.21)$$

Where  $lat = 35.902^\circ$  is latitude of the Kashiwa ground station,  $lon = 139.935^\circ$  is the longitude of the Kashiwa ground station,  $R_E = 6378.137$  (km) is the mean equatorial radius of the Earth.

The Az-El angle and the distance R between satellite and Kashiwa ground station are calculated as in Formula 2.22-2.24.

$$Az = \arccos\left(\frac{Y}{\sqrt{Y^2 + Z^2}}\right) \quad (2.22)$$

$$El = \arctan\left(\frac{Z}{\sqrt{X^2 + Y^2}}\right) \quad (2.23)$$

$$R = \sqrt{X^2 + Y^2 + Z^2} \quad (2.24)$$

The Az-El angle and distance R calculated here with the time  $t_k$  will be written to the antenna schedule file (mentioned in chapter 2.2.2). Additionally, it should be noted that

when using this method to calculate the satellite position forecast, the interval between the calculated time and the epoch time of the TLE data should preferably not be more than 7 days in order to avoid a massive error between the calculation result and the actual satellite position.

### 2.3.2 Real-time automatic tracking method

Because it is hard to eliminate computational errors from satellite prediction calculations, the Kashiwa ground station performs real-time automated alignment in addition to program tracking (tracking based on the forecasted satellite position schedule). The real-time automatic alignment is realized by the Advanced-step-tracking Method developed by Astrocub Inc..

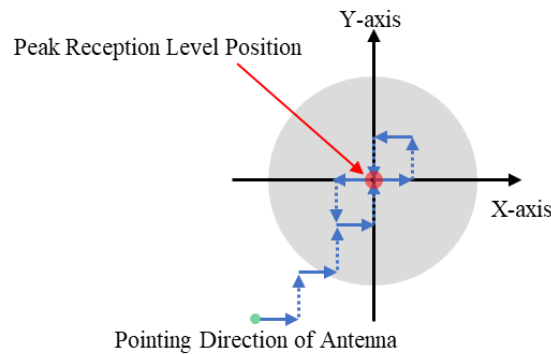


**Figure 2.30 Conceptual diagram of the Advanced-step-tracking Method**

Figure 2.30 illustrates the basic idea behind the Advanced-step-tracking Method. When the actual position of the satellite has an inevitable error with the calculated position, the antenna will move the two axes slightly and judge the change in the received signal to approach the actual position of the satellite step by step.

It should be noted that the standard step-tracking method is usually used for geostationary(GEO) satellites. Antennas are capable of automatically locating satellite positions when provided a starting direction. Only the approximate beginning position is calculated in this method; the satellite position over time (schedule) is not required.

In contrast, Advanced-step-tracking method is used for LEO satellites. It is based on program tracking, and at the same time, the antenna is slightly shifted by an angle to gradually find the actual position of the satellite. Figure 2.31 shows the effect of the Advanced-step-tracking method, reflecting the gradual process of finding the satellite's actual position.

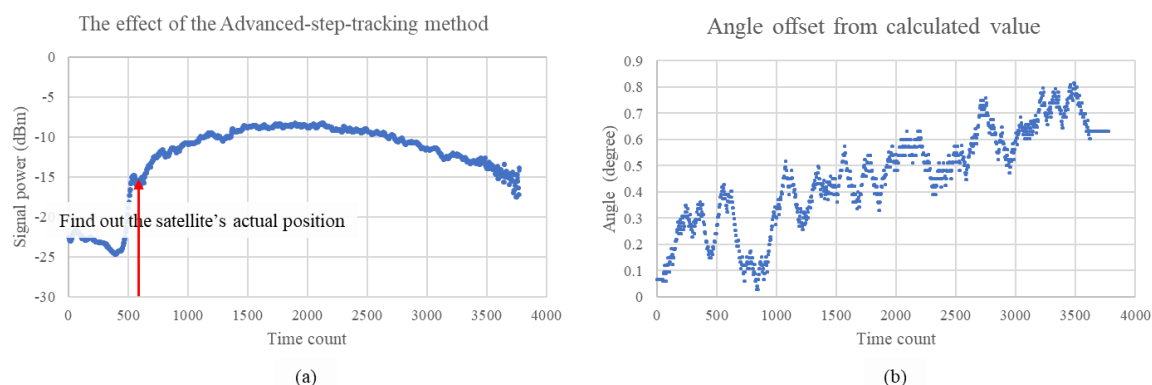


**Figure 2.31 The effect of the Advanced-step-tracking method: (a) variation in received signal strength (b) error between the actual satellite position and the calculation**

This function is implemented by ACAutoTrack1.exe. Figure 2.32 shows the screenshot of the ACAutoTrack1.exe window.

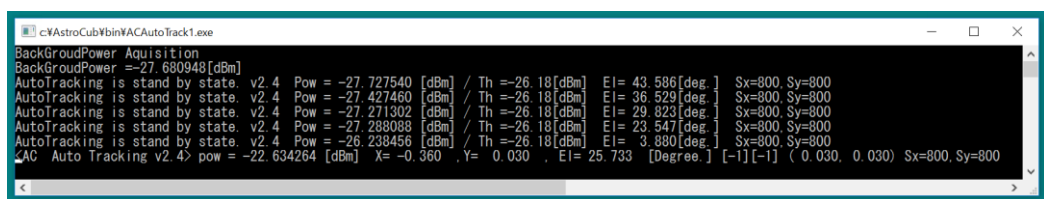


**Figure 2.32 The window of ACAutoTrack1.exe**

The specific functional flowchart of ACAutoTrack1.exe is shown in Figure 2.33.

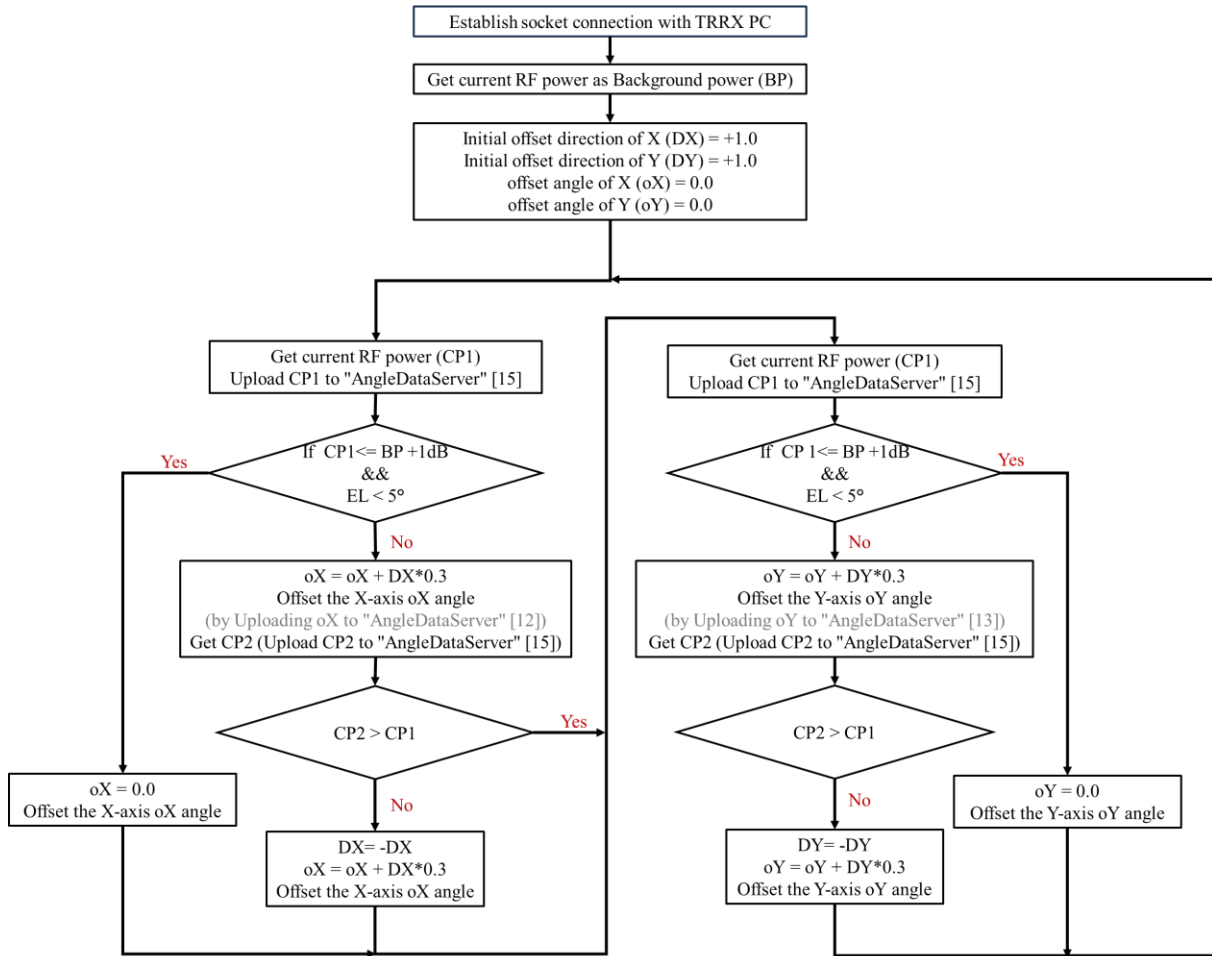


**Figure 2.33 The functional flowchart of ACAutoTrack1.exe**

When tracking the satellite, ACAutoTrack1.exe uploads the judgment of the offset angle to "AngleDataServer" [12] [13], and the antenna will be oriented in the direction of  $(aX, aY) = ([8] + [12], [9] + [13])$ . It is crucial to remember that the ACAutoTrack1.exe needs to be running in order to read data about signal strength from the TRRX PC. Otherwise, the shared memory "AngleDataServer" [15] in the antenna PC cannot be updated with new signal strength information.

## 3. Performance evaluation for Kashiwa ground station

### 3.1 True north calibration

#### 3.1.1 Description

An azimuth angle inaccuracy will result when the antenna is physically mounted to the ground station. As described in Chapter 2.1.2, when calculating the X-Y antenna aX-aY angle and Az-El angle conversion, the antenna's X-axis needs to be overlapped with the direction of north. However, it is unavoidable that there will be an angle between the X-axis and the north during the actual installation (as shown in Figure 3.1).

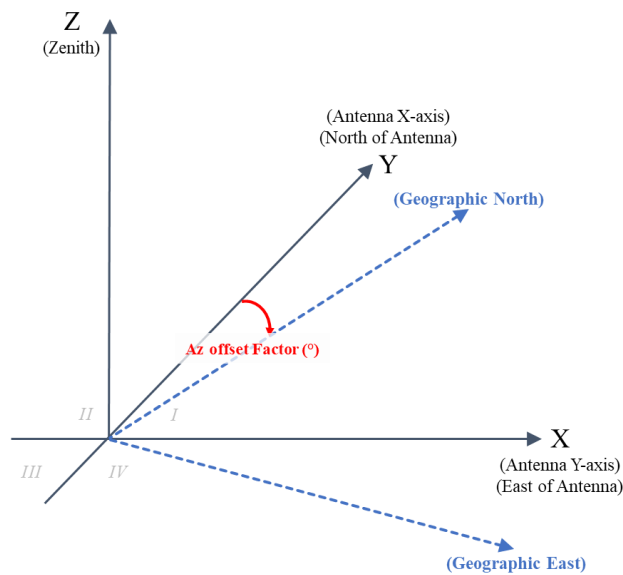


**Figure 3.1 The reason for the requirement of north calibration**

The Az offset factor is defined as the angle between the geographic north and the antenna X-axis. When the antenna is tracking according to the schedule, the Az angle in the schedule should be corrected ( $Az = Az + Az\_offset\_factor$ ) before being converted into the aX-aY angle. In order to correctly point the antenna towards the satellite during

tracking, the Az offset factor of the antenna needs to be measured.

### 3.1.2 Measurement method

For measurements, a stable and well-calculated positional solar signal will be used. As shown in Figure 3.2, the antenna will be fixed by being pointed toward where the sun will be at time  $t_0$  and offset by an angle in the azimuth direction. The received signal strength is monitored for thirty minutes, starting 15 minutes before  $t_0$  and ending 15 minutes after  $t_0$ . From the variation of the received signal over time, determine whether the offset angle is an appropriate Az offset factor.

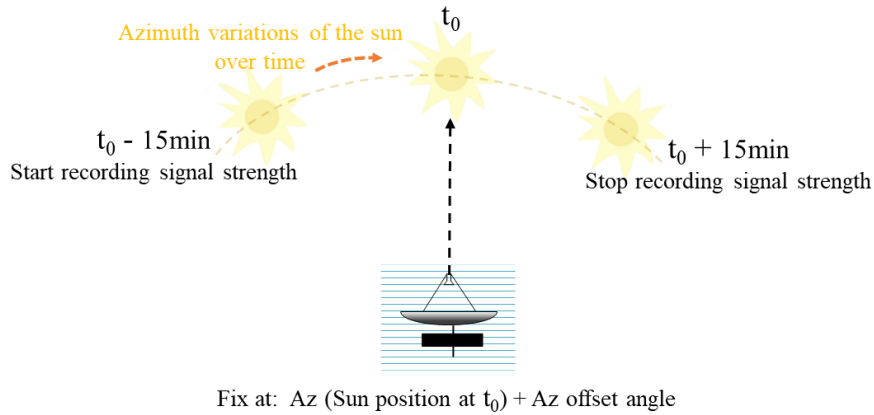


**Figure 3.2 Conceptual diagram for measuring Az offset factor**

The received signal will reach its maximum strength when the antenna is positioned in the azimuth of the sun's position. Therefore, if the peak signal strength occurs after  $t_0$  (as in Figure 3.3(a)), it means that the antenna is pointing at an azimuth greater than the azimuth of the sun's position at  $t_0$ , so the Az offset angle needs to be adjusted smaller. On the other hand, if the peak signal strength occurs before  $t_0$ , the Az offset angle should be adjusted to a larger angle. When the peak signal strength occurs at the time of

to (as in Figure 3.3(b)), the az offset angle is set as the ideal Az offset factor.

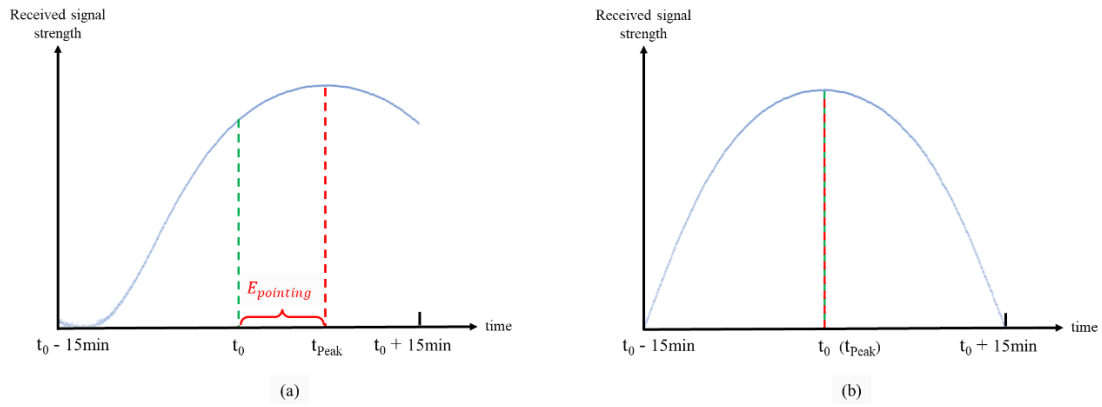


**Figure 3.3 Example of received signal variation with time for different Az offset angle:**  
**(a) excessive Az offset angle (b) ideal Az offset factor**

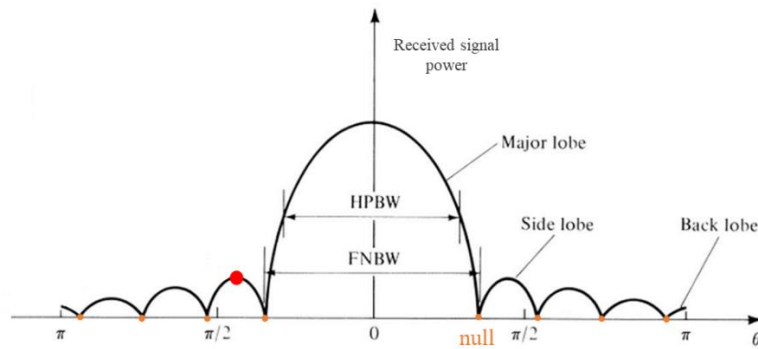
The advantage of using the sun for the true north calibration is that it may be accurately measured without setting up additional signal sources or other equipment. Additionally, even though the measurement method described in this chapter is time-consuming, the results are highly reproducible.

## 3.2 Power pattern

### 3.2.1 Description

An antenna is a converter that transforms an electromagnetic wave propagating in free space into a guided wave propagating on a transmission line when it is used for reception. However, when the same signal source is situated in different directions of the antenna in space, the receiving antenna's capacity to transform electromagnetic waves from the source differs. In other words, the received signal power of the antenna is different when the source is located in different directions from the antenna in space.

The power pattern describes the distribution of the antenna's normalized received signal power in two or three dimensions. It can be used to represent the antenna's reception performance and indicate the antenna's sensitivity in different directions of the antenna.



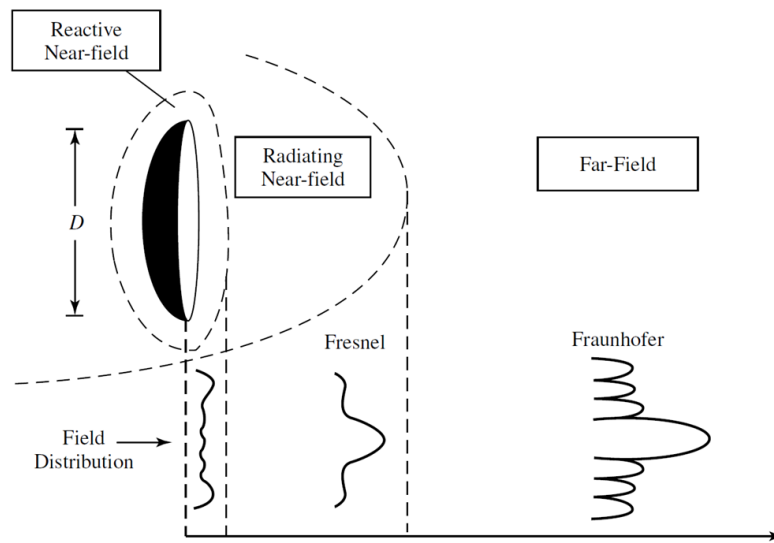
**Figure 3.4 Linear 2-D plot of power pattern (Constantine A., 2005)**

Figure 3.4 shows a linear 2-dimensional power pattern depicting the variation of received signal power with the angle between the signal source and the antenna. (The source is located in a specific spatial plane and is equally far from the antenna. ) The point where the power value is 0 is called the null point. The angular region between two adjacent null points with the largest peak value is referred to as the major lobe, and others are referred to as the side lobe. The following are the most typical metrics used to describe the power pattern:

- Half power beamwidth (HPBW): the angular range of more than half of the major lobe's peak power
- Side lobe level (SSL): the maximum value of side lobes

A narrow HPBW and a low SSL are necessary for a directional antenna to be able to receive a specific signal source coming from that direction while suppressing sources of interference coming from other directions.

The area around the antenna can be divided into three regions, and the shape of the power pattern changes continuously with distance from the antenna until the far-field region. In the far-field region, the relative angular distribution of the field is independent of the distance from the antenna, and the major lobe, side lobe, and null points of the power pattern have all been formed (as in Figure 3.5).



**Figure 3.5 Typical changes of power pattern shape in different regions of the antenna (Constantine A., 2005)**

The antenna's design specifications are typically created for far-field applications (such as satellite communications). As a result, the far-field region is a crucial field for antenna testing, and measurements of the antenna's different properties, including the power pattern, must be performed in this region.

### 3.2.2 Measurement method

The most basic way to measure the power pattern is to place a signal source in the antenna's far-field region, then rotate the antenna in a particular plane so that the

antenna and the source have an angular difference ( $\theta$ , as shown in Figure 3.6). The power pattern is a linear graph generated by continuously changing the value of theta and noting the strength of the associated received signal.

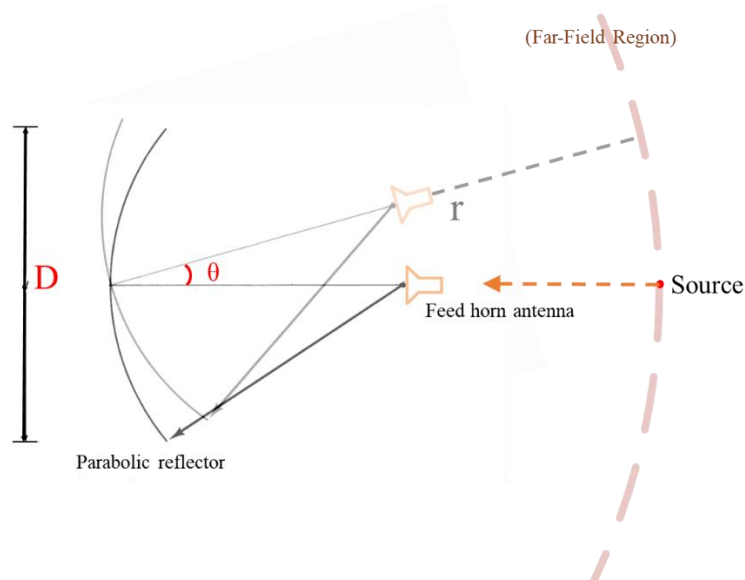


**Figure 3.6 Conceptual diagram for measuring power pattern**

The far-field region of the antenna can be calculated as in Formula 3.1.

$$r > \frac{2D^2}{\lambda} \quad (3.1)$$

Where  $D$  is the diameter of the antenna,  $\lambda$  is the wavelength of the received signal.

When receiving S-band signals, the 2.4 m antenna's far-field area must satisfy  $r > 86.4\text{m}$ , and when receiving X-band signals, it must satisfy  $r > 312\text{m}$ . The Kashiwa ground station is located in the center of the campus, with no open space in its immediate vicinity. It is not easy to place the signal source in a location that satisfies the distance conditions. Furthermore, the ground reflection will enormously impact the final result.

As a result, picking a signal source in the sky, like the sun or a satellite, should be considered. Since the apparent size of the sun is 0.53 degrees, the results of beamwidth will be slightly larger when using the solar signal to measure the power pattern. In this measurement, the satellite was used as a signal source.

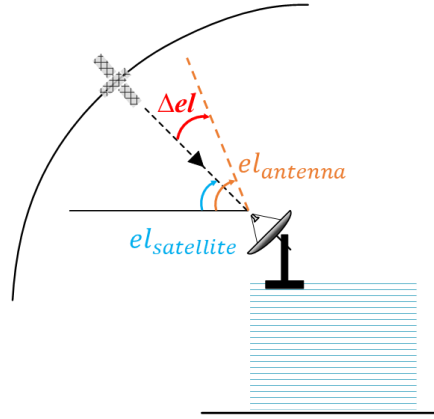


**Figure 3.7 Power pattern measurement using the satellite signal as a signal source**

As shown in Figure 3.7, the antenna is offset by an  $\Delta el$  angle in the El direction while tracking the satellite, and the strength of the received signal is recorded. The pointing of the antenna is shown by Formula 3.2.

$$el_{antenna(t)} = el_{satellite(t)} + \Delta el_{(t)} \quad (3.2)$$

Where  $\Delta el_{(t)}$  is a time-related function, it changes linearly with time over a range.

### 3.3 G/T (Gain to Noise Temperature)

#### 3.3.1 Description

In order to get the image data from Earth observation satellites (Figure 3.8), the ground station receiving system needs to process the signal into the appropriate frequency and

intensity before sending them to the demodulator for demodulation. To accurately produce these images throughout this process, the received data must have a low bit error rate (BER). Therefore the ground station is required to have the significant ability to enhance the satellite signal without amplifying the noise signal.

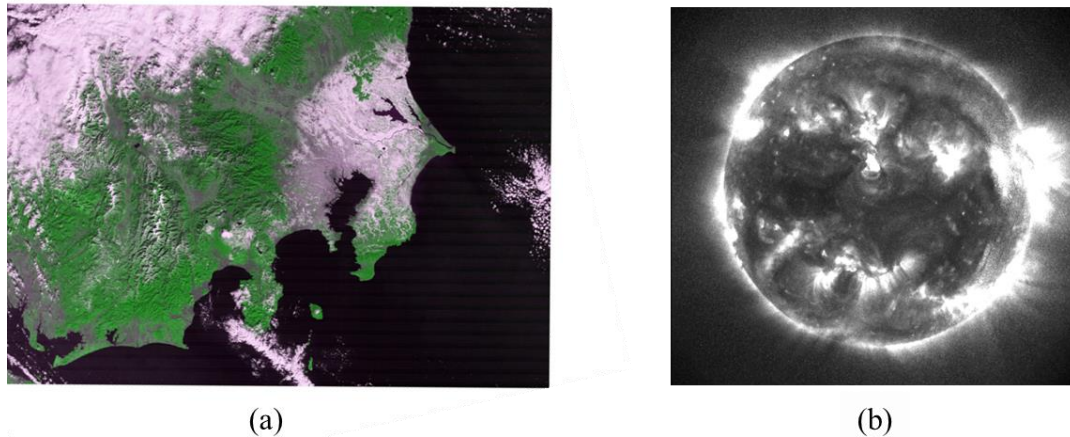


**Figure 3.8 Images received by Kashiwa ground station:**  
**(a) earth's surface image received by Terra (b) solar image received by Fengyun 3E**

The performance of a ground station receiving system is evaluated by the G/T metric.

- G: The antenna gain, the ability of the antenna to amplify the received signal.
- T: The noise temperature of the receiving system, which is the equivalent temperature of the noise-induced thermal movement of electrons in the receiving system.

The receiving system has two different types of noise sources (as in Figure 3.9). They are the noise from the environment and the noise generated in the circuitry of the receiving equipment.

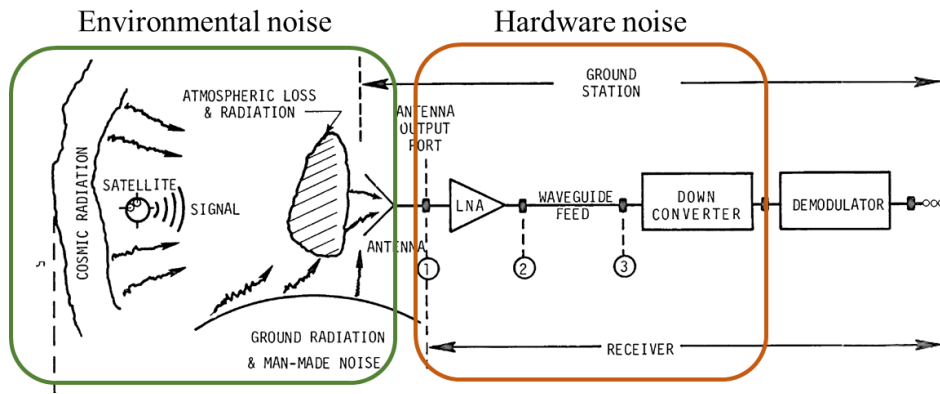


**Figure 3.9 Occurrence of noise in a ground station's receiving system (D. F. Wait, 1974)**

It is important to note that ground stations are generally chosen to be built in open areas with less man-made noise. However, the Kashiwa ground station is located in the middle of campus, so the noise from the surrounding environment cannot be ignored. Figure 3.10 shows the scanning results of the environmental noise around the Kashiwa ground station (scanning area: Az: 0°-180°, El: 3°-28°).

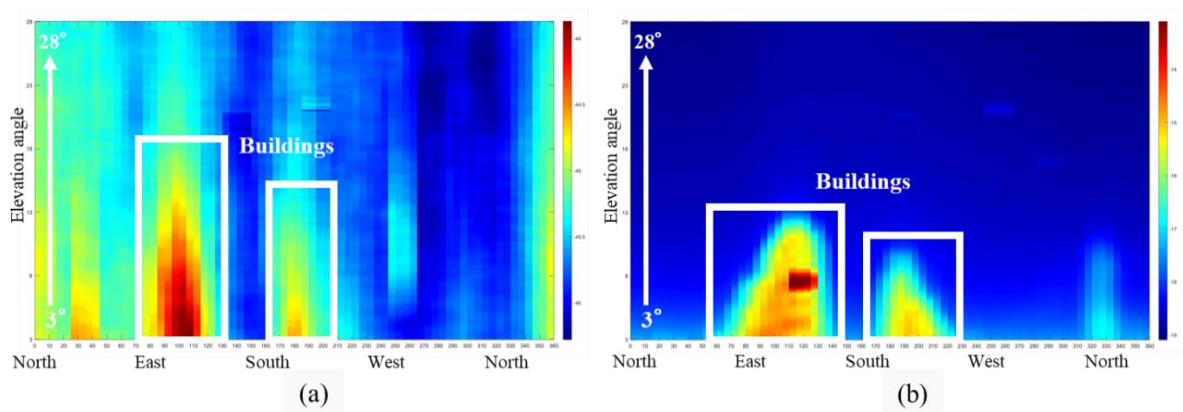


**Figure 3.10 Environmental noise signal around Kashiwa ground station:  
(a) S band: 2.25 GHz (b) X band: 8.2 GHz**

As shown in Figure 3.10 (a), the noise from nearby buildings, cell phone base stations, and towers can be picked up in the S-band. As shown in Figure 3.10 (b), the noise in the X-band mainly comes from buildings. In order to take into account the effects of these

actual installation environments, it is crucial to conduct performance tests after the antenna has been placed.

G/T is the ratio of the ground station's ability to amplify the received signal to the amount of noise in the receiving system. A ground station with a high G/T can reduce the loss of received data and lower the BER when receiving weak signals.

### 3.3.2 Measurement method

The Y-factor method was used for this G/T measurement. The basic idea is to connect two signal sources with varying temperatures to the device (or system) under test, and the input noise power from the source to the device is measured with a power meter (as in Figure 3.11).

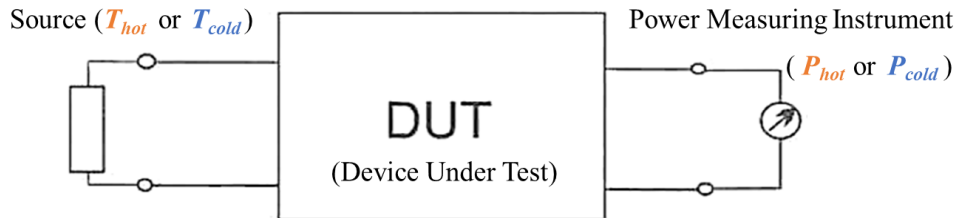


**Figure 3.11 Conceptual diagram for Y - factor method (S. Cakaj, 2005)**

The theoretical calculation of the input noise powers is shown in Formula 3.3.

$$P = k(GT_{source} + T_{dut})B \quad (3.3)$$

Where  $k = 1.38 \times 10^{-23}$  J/K is the Boltzmann constant, G is the gain of the device under test,  $T_{source}$  is the temperature of the source,  $T_{dut}$  is the noise temperature of the device under test, B is the spectral bandwidth of the power measurement.

The ratio of the two measured input noise powers is the Y-factor, as in Formula 3.4.

$$Y = \frac{P_{hot}}{P_{cold}} = \frac{k(GT_{hot} + T_{dut})B}{k(GT_{cold} + T_{dut})B} \quad (3.4)$$

Therefore, the G/T value of the device under test can be obtained from the two measured input noise powers and the Y factor as in Formula 3.5.

$$\frac{G}{T_{dut}} = \frac{Y - 1}{T_{hot} - YT_{cold}} \quad (3.5)$$

In measuring the G/T of the Kashiwa ground station receiving system, the sun and the sky are used as two signal sources (as in Figure 3.12).

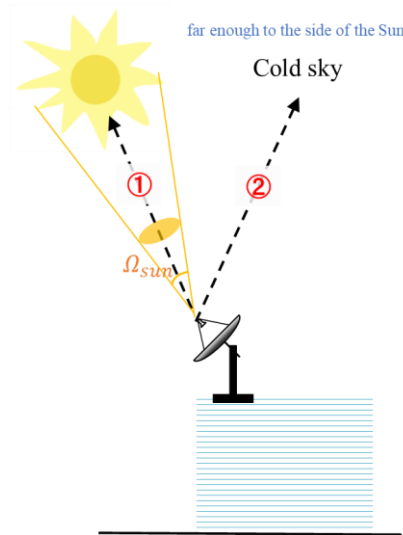


**Figure 3.12 Conceptual diagram for using the Sun as a source to measure G/T**

By first pointing the antenna to the sun position, the theoretical calculation of the received power is as in Formula 3.6.

$$P_{sun} = k(GT_{sun} \frac{\Omega_{sun}}{4\pi} + T_{system})B \quad (3.6)$$

Where G is the gain of the antenna,  $T_{sun}$  is the temperature of the sun,  $\Omega_{sun}$  is the solid angle of the sun,  $T_{system}$  is the noise temperature of the receiving system, B is the spectral

bandwidth of the power measurement.

By pointing the antenna toward the cold sky far enough from the sun, the theoretical calculation of the received power is as in Formula 3.7.

$$P_{cold\_sky} = kT_{system}B \quad (3.7)$$

So the G/T of the system can be derived from the Y-factor as in in Formula 3.8.

$$\frac{G}{T_{system}} = \frac{4\pi(Y-1)}{T_{sun}\Omega_{sun}} \quad (3.8)$$

Where  $Y = P_{sun}/P_{cold\_sky}$  is Y-factor.

However, the Sun's temperature varies significantly in different wavelengths (as in Figure 3.13). In the optical range, the Sun can be thought of as a blackbody with a constant temperature of 6000 K. In the radio frequency band, the equivalent temperature for a disturbed Sun is dramatically different from that for a quiet Sun.

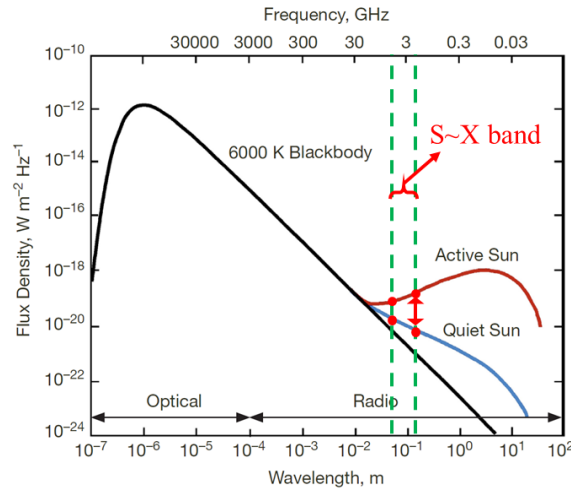


**Figure 3.13 The solar radiation spectrum at optical and radio frequencies (C. Ho, 2008)**

Therefore, in the calculation of G/T, the solar temperature at the received frequency is calculated from the amount of solar flux density. Solar flux density is a measure of the

amount of solar energy received per unit area per unit of time at a particular location in space. The solar temperature at the received frequency is calculated as in Formula 3.9.

$$T_{sun} = \frac{1}{2} \frac{F_{sun} \lambda^2}{k \Omega_{sun}} \quad (3.9)$$

Where  $F_{sun}$  ( $10^{-22} \text{ W} \cdot \text{m}^{-2} \cdot \text{Hz}^{-1}$ ) is the solar flux density,  $\lambda$  (m) is the wavelength of the received signal. The factor 1/2 accounts for the fact that only one polarization of radiation can be received from the sun at any one time.

Because solar energy radiation varies greatly with solar activity, we used solar flux density data provided by NOAA for this calculation. The data will provide the daily noon solar flux density for the area where each solar station is located. In this study, we used data from the Learmonth station in Australia.

#Current Space Weather Indices			
:Solar_Radio_Flux: 2023 Mar 23			
#	Learmonth	San Vito	Sag Hill
#	0400	1000	1700
245	32	-1	-1
410	45	-1	-1
610	62	-1	-1
1415	108	105	-1
2695	138	-1	-1
2800	-1	-1	-1
4995	180	158	-1
8800	291	261	-1
15400	574	564	-1

**Figure 3.14 Example of NOAA solar flux data**

( **Data from** <https://services.swpc.noaa.gov/text/current-space-weather-indices.txt> )

As shown in Figure 3.14., the first column shows the frequency (MHz) at which the solar flux density was measured, and the second column shows the solar flux density measured at Learmonth station. A ‘-1’ means that a value has not been measured for that time and frequency. The frequencies provided by this data are not continuous, but the solar flux density at the desired frequency can be calculated by interpolation, as

shown in Formula 3.10-3.11.

$$I_e = \frac{\log_{10}\left(\frac{f_{GT}}{f_2}\right)}{\log_{10}\left(\frac{f_1}{f_2}\right)} \quad (3.10)$$

$$F_{f_{GT}} = F_{f_2} \left( \frac{F_{f_1}}{F_{f_2}} \right)^{I_e} \quad (3.11)$$

Where  $I_e$  is the interpolation exponent,  $f_{GT}$  is the frequency in the G/T measurement,  $f_1$  and  $f_2$  are the frequencies in the data ( $f_1 < f_{GT} < f_2$ ),  $F_{f_{GT}}$  ( $10^{-22} \text{ W} \cdot \text{m}^{-2} \cdot \text{Hz}^{-1}$ ) is the solar flux density at the frequency in the G/T measurement,  $F_{f_1}$  and  $F_{f_2}$  are the solar flux density provided in data at  $f_1$  and  $f_2$  frequencies.

Since the Sun is not a point source, the antenna receives signals not only from the peak of its radiation pattern, but also from points on the pattern with less than maximum gain. Therefore, the theoretical value of the received solar signal power is lower than the calculated value in Formula 3.6 and should be multiplied by the beam correction factor C, as in Formula 3.12-3.13.

$$P_{received\_sun} < P_{sun} = k(GT_{sun} \frac{\Omega_{sun}}{4\pi} + T_{system})B \quad (3.12)$$

$$P_{received\_sun} = k(GT_{sun} \frac{\Omega_{sun}}{4\pi} \cdot C + T_{system})B \quad (3.13)$$

The beam correction factor C is calculated as in Formula 3.14-3.16.

$$C = \frac{1 - \exp\left[-\left(\frac{r}{B_w}\right)^2 \cdot \ln(2)\right]}{\left(\frac{r}{B_w}\right)^2 \cdot \ln(2)} \quad (3.14)$$

$$r = 0.525(1.24 - 0.162 \log_{10} f_{GT}) \quad (3.15)$$

$$B_w = 68 \frac{\lambda}{D} \quad (3.16)$$

Where  $r$  is the effective RF diameter of the sun in degree, the factor 0.525 is the apparent angular diameter of the sun in degree,  $f_{GT}$  (GHz) is the frequency in the G/T measurement,  $B_w$  is the HPBW of the antenna in degree,  $\lambda$  (m) is the wavelength of the received signal,  $D=2.4$ (m) is the diameter of the antenna.

Combining Formulas 3.8, 3.9, 3.11, and 3.13, the receiving system G/T in dB/K is calculated as in Formula 3.17.

$$\frac{G}{T_{system}} = 10 \log_{10} \left[ \frac{8\pi k(Y-1)}{F_{f_{GT}} \lambda^2 C} \right] \quad (3.17)$$

Note that the Y-factor in Formula 3.17 is in linear representation and is calculated as in Formula 3.18.

$$Y = 10^{\frac{P_{sun} - P_{cold\_sky}}{10}} \quad (3.18)$$

Where  $P_{sun}$  (dB) is the power received by the antenna system when pointed at the sun,  $P_{cold\_sky}$  (dB) is the power received by the antenna system when pointed at the cold sky (at the same elevation as  $P_{sun}$ ).

## 4. Results and Discussions

### 4.1 True north calibration

The manufacturing company had done a rough north calibration when the Kashiwa ground station was first established. The Az offset factor was set to  $+12.0^\circ$  for the S-band antenna and  $-9.1^\circ$  for the X-band antenna. Based on the original Az offset factor, the true north calibration experiment was re-conducted, and the results are shown in Figure 4.1.

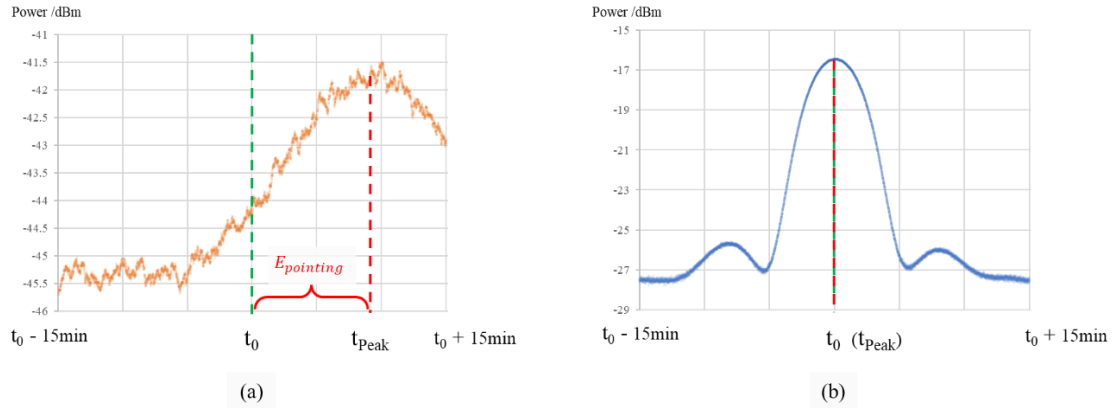


**Figure 4.1 Current status of true north calibration for Kashiwa ground station:**  
**(a) S band, Az offset factor =  $+12.0^\circ$  (b) X band, Az offset factor =  $-9.1^\circ$**

As shown in Figure 4.1(a), The S-band antenna is not aligned to true north by the current Az offset factor. While the x band antenna, as shown in Fig. 4.1(b), accurately finds the geographic position of the sun and therefore completes the calibration of true north.

In order to find a suitable Az offset factor for S-band, the Az offset angle is continuously adjusted for the true north experiments. The pointing error of the sun's

position ( $E_{\text{pointing}} = t_{\text{peak}} - t_0$ ) is calculated, and the results are shown in Figure 4.2.

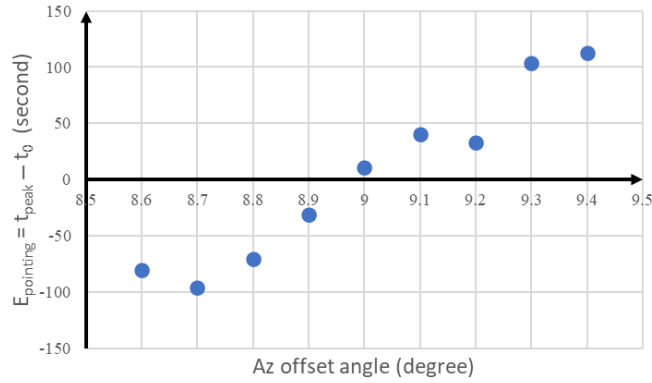


**Figure 4.2 Relationship between Az offset angle and pointing error**

As shown in Figure 4.2, the absolute value of the sun's pointing error reaches a minimum at an Az offset angle of  $9^\circ$ . Even though all measurements were taken on the same day, the experiment's long measuring period caused the sun's position to shift significantly. As a result, the measurement was not entirely linear. From this experimental result, the Az offset factor of the S-band antenna should be set to  $9^\circ$ .

## 4.2 Power pattern

The advantage of using satellite signals as a signal source is that it can reduce the interference caused by ground reflection and other man-made factors. However, it also has the drawback of instability. As shown in Figure 4.3, for the same satellite, the stability of the signal strength as it passes through the ground station each time also has a big difference. In (a), the signal strength is more stable and varies with the distance from the satellite ground station. In (b), the signal strength is erratic and unexpected.

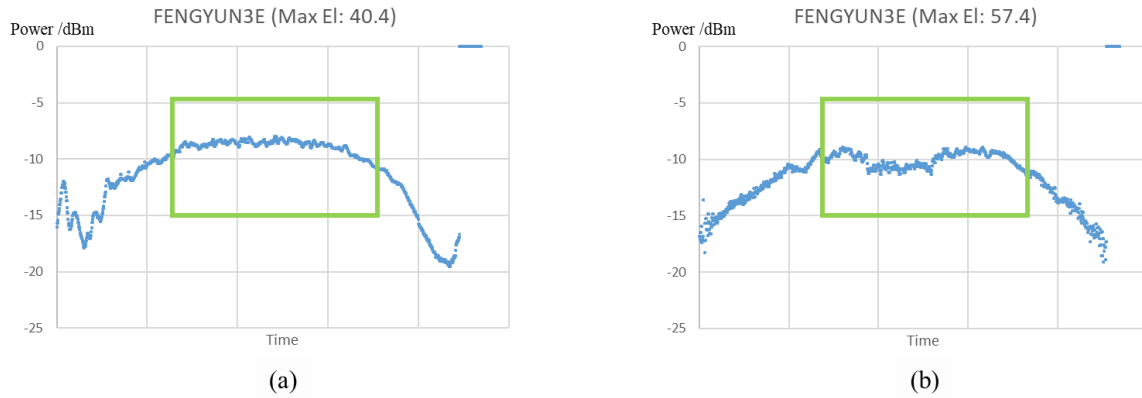


**Figure 4.3 Record of received signal strength over time:**  
**(a) stable condition (b) unstable condition**

When the unstable satellite signal is used to measure the power pattern, the measured power pattern will be inaccurate (the beamwidth will be significantly wider or narrower), and it is possible to obtain the result, as shown in Figure 4.4.

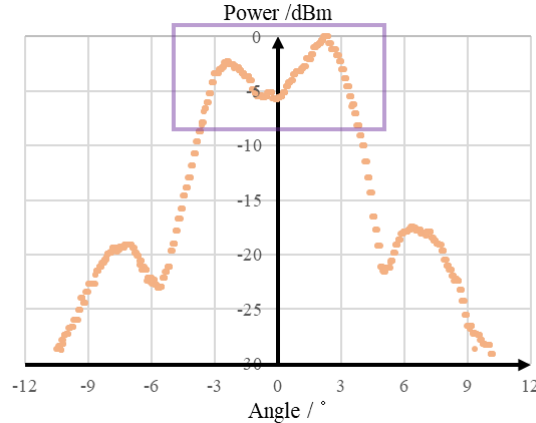


**Figure 4.4 Unusual measurement result for the power pattern**

The measurement result in Figure 4.4 may also be the consequence of inaccurate satellite position prediction calculations, which prevent the antenna from pointing to the satellite at the anticipated offset angle. Therefore, it is necessary to choose a satellite with a more stable signal as the signal source and make several measurements to select the better result.

Figure 4.5 shows a better set of measurement results of the power pattern.

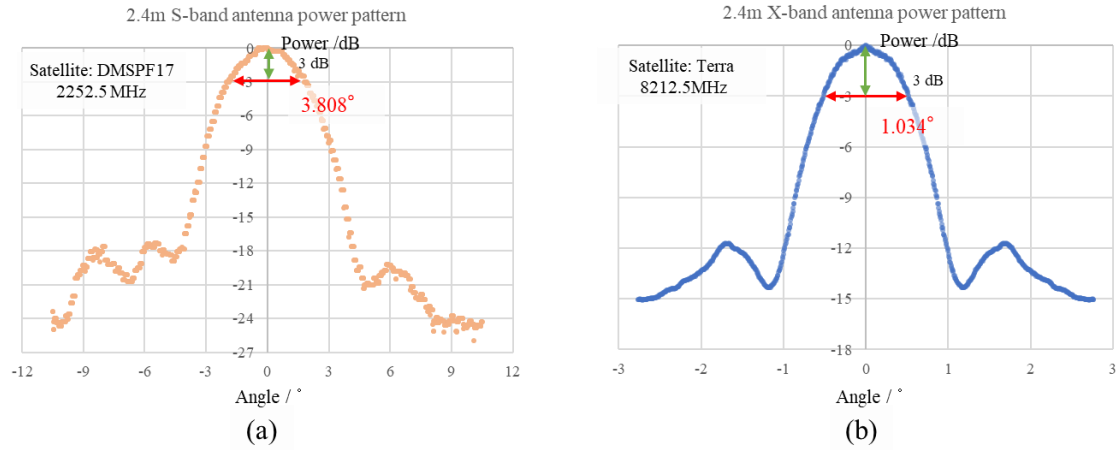


**Figure 4.5 Measurement results for the power pattern: (a) S-band (b) X-band**

The S-band antenna's power pattern was measured using the DMSP satellite at 2252.5 MHz. According to the measurement results (Figure 4.5(a)), the HPBW is 3.81°, and the SSL is -17.4 dB. The X-band antenna's power pattern was measured using the TERRA satellite at 8212.5 MHz. According to the measurement results (Figure 4.5(b)), the HPBW is 1.03°, and the SSL is -11.7 dB. The results show that the same-size antenna has stronger directivity in receiving signals in X-band.

### 4.3 G/T (Gain to Noise Temperature)

The sun's passing path is relatively constant from day to day. Figure 4.6 shows the sun's position in relation to the Kashiwa ground station on 2023/06/30.

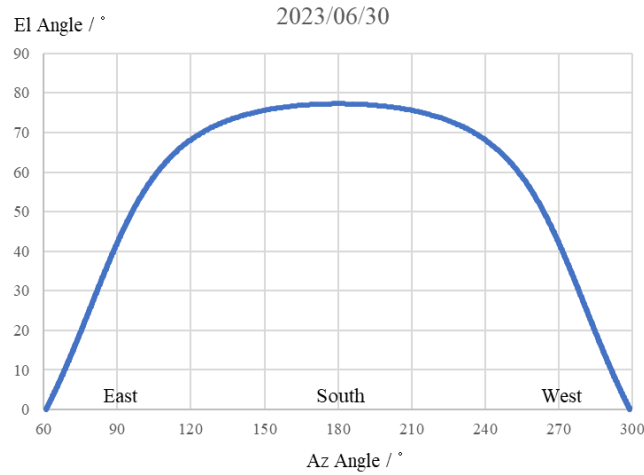


**Figure 4.6 Sun position relative to the Kashiwa ground station on 2023/06/30**

Although obtaining the effect of environmental noise on the antenna G/T is desirable, measurements using the sun as a signal source can only measure G/T values in the direction of the sun's passage. As shown in Figure 4.6, the sun's path can be divided into two sections: from sunrise to noon (Az angle:  $60^{\circ}\sim 180^{\circ}$ ) and from noon to sunset (Az angle:  $180^{\circ}\sim 300^{\circ}$ ). In this study, G/T measurements used the sun position mainly from the noon to sunset period.

Specifically:

1. tracking the sun's position for one hour and receiving the sun signal
2. tracking the sky signal using the same path as Step 1
3. repeat Steps 1 and 2 until sunset.

It is worth noting that the one-hour intervals, alternating between tracking the sun and the sky, ensured that the sun had moved far enough away by the time receiving the sky signal.

The results of the X band receiving system's measurements of the sun and sky signals are shown in Figure 4.7.

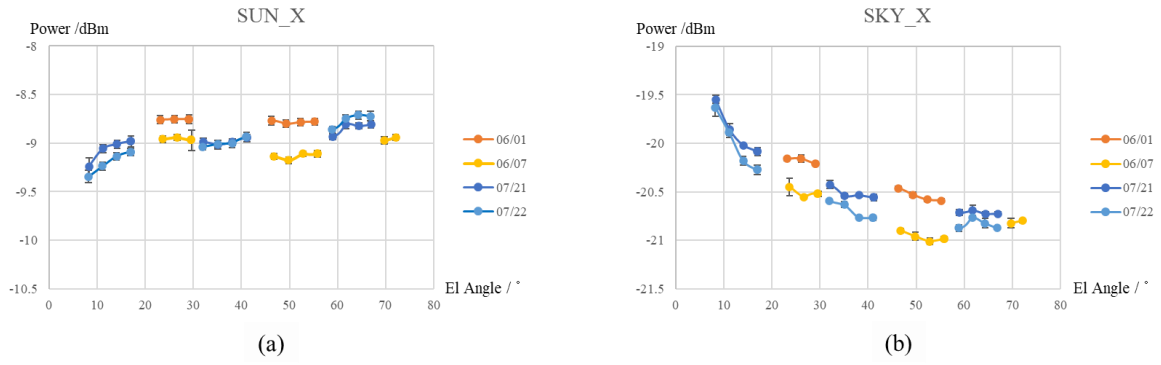


**Figure 4.7 Variation of solar and sky signals with elevation angle measured by the X band receiving system: (a) solar signal (b) sky signal**

As shown in Figure 4.7(a), the solar signal is slightly reduced at low elevation angles ( $El < 10^\circ$ ). This is because solar radiation travels a longer distance through the atmosphere at low elevations, resulting in more attenuation of the solar radiation by the atmosphere. As shown in Figure 4.7(b), the sky noise gradually increases with decreasing elevation angle, resulting from man-made noise sources such as various buildings near the ground. The results of the Y-factor calculated from the measurements are shown in Figure 4.8.

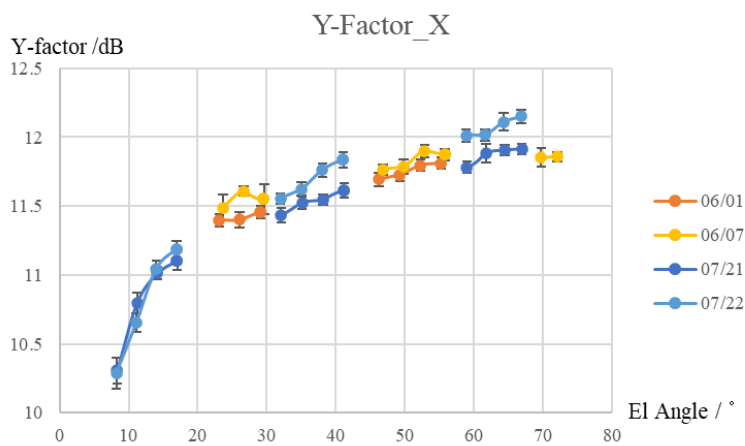


**Figure 4.8 The Y-factor calculated from the X band receiving system measurements**

The Y-factor shows the difference between the solar signal and the sky signal. As

shown in Figure 4.8, there is a clear tendency for the Y-factor to decrease as the elevation angle decreases. The G/T values of the X band receiving system calculated by the Y-factor are shown in Figure 4.9.

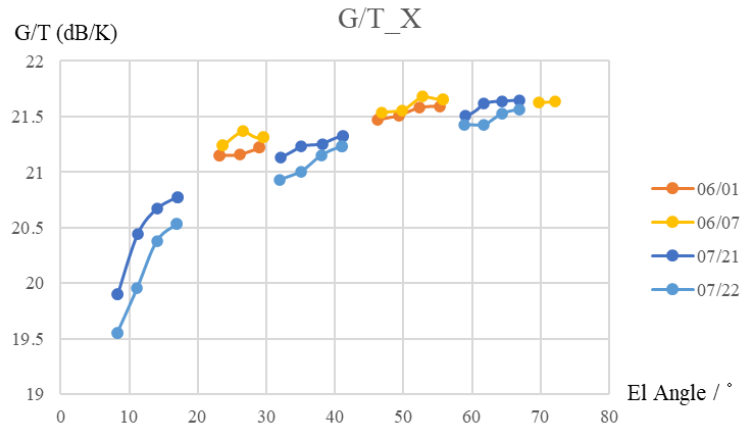


**Figure 4.9 The G/T value calculated from the X band receiving system measurements**

As shown in Figure 4.9, at high elevation ranges ( $El > 45^\circ$ ), the G/T value of the X band receiving system is around 21.5 dB/K. As the elevation angle decreases, the G/T value will gradually decrease to about 19.5 dB/K. In general, the G/T value for ground stations is expected to be 10 dB/K or greater. Therefore, the X band receiving system of the Kashiwa ground station has a sufficiently high performance.

For the S band receiving system, the measurements of the sun and sky signals are shown in Figure 4.10.

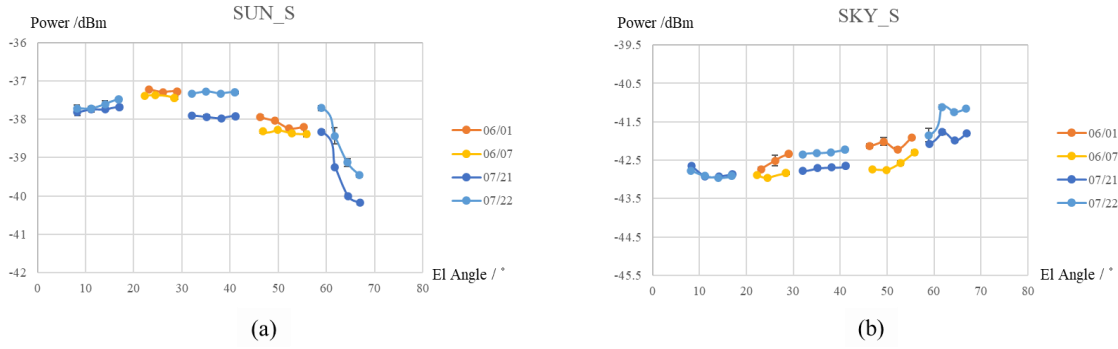


**Figure 4.10 Variation of solar and sky signals with elevation angle measured by the S band receiving system: (a) solar signal (b) sky signal**

As shown in Figure 4.10(a), measurements of the solar signal provide unexpected results. In contrast to the measurement result of the X band (Figure 4.7(a)), the solar signal strength rapidly declines at an elevation angle of roughly 60°. The reason for this result has yet to be explored. As shown in Figure 4.10(b), unlike the variation of the sky noise under the X band, the sky noise under the S band increases with increasing elevation angle. The main reason here is that the path of measuring the sky noise is the same as the path of measuring the solar signal, and the orientation of the sun when it is in the high elevation region has several radio equipments as sources that emit signals in the S band, which leads to the sky noise becoming greater. The results of the Y-factor calculated from the measurements are shown in Figure 4.11.

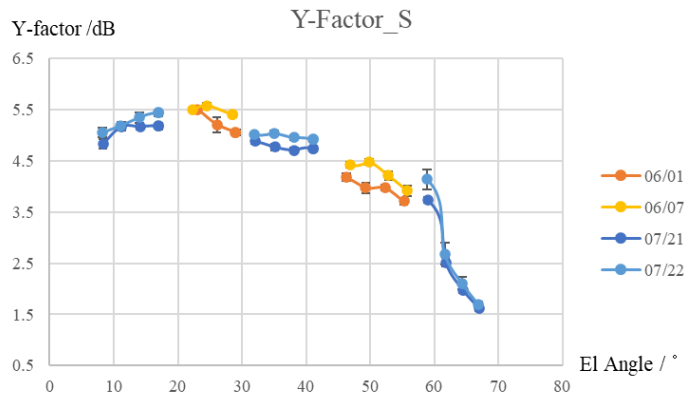


**Figure 4.11 The Y-factor calculated from the S band receiving system measurements**

In Figure 4.11, the decrease of the Y-factor in the region of elevation angles between  $40^{\circ}$ ~ $60^{\circ}$  is due to environmental noise. In the region with elevation angles above  $60^{\circ}$ , the decrease of the Y-factor is brought on by a dramatic decline in the solar signal. Since the reason for the drop of the received solar signal is unknown, the G/T values in the high elevation angle region are not calculated for the time being. The G/T values of the S band receiving system calculated by the Y-factor are shown in Figure 4.12.

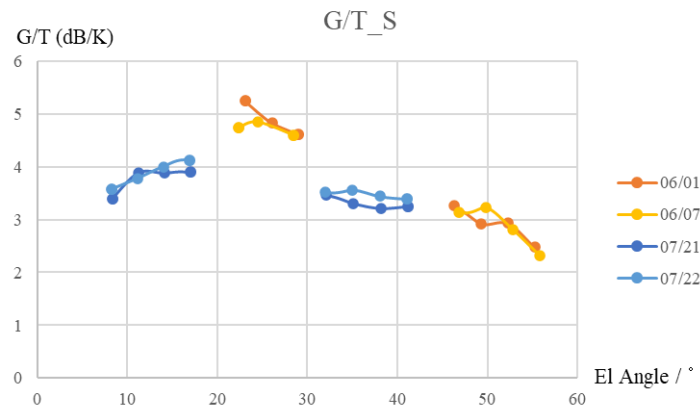


**Figure 4.12 The G/T value calculated from the S band receiving system measurements**

As shown in Figure 4.12, the G/T value of the S-band receiving system is about 3-5.5 dB/K in the area with an elevation angle below  $50^{\circ}$ . In the area with elevation angle above  $50^{\circ}$ , the G/T value decreases to about 2 dB/K with the increase of elevation angle. Therefore, the ability to receive satellite signals is relatively weak for the S-band receiving system. This will result in a lower reception signal-to-noise ratio when receiving satellites with weaker transmit power, making extracting useful information from the noise difficult. It will also face a greater impact on the received signal from environmental interference, such as solar activity.

## 5. Summary

Satellite utilization is gradually becoming civilized with the gradual maturation of satellite manufacturing and launch technologies. In order to better utilize the information brought by satellite data, the demand for highly automated and low-cost satellite ground stations will increase dramatically. This study is based on the Kashiwa ground station constructed by Astrocub Inc. to prepare for the joint satellite operation with Taiwan ground station in the near future. The main work involved in this thesis includes:

1. A thorough overview of the Kashiwa ground station's hardware and software system architecture is provided. In addition, a straightforward model for calculating satellite location using TLE data was developed, and the fundamentals of the real-time position correction method were clarified. These will create a solid basis for the Kashiwa ground station's continued renovation.
2. Three critical performance evaluations of the ground station are discussed, including the true north calibration, the power pattern of the antenna, and the G/T value of the receiving system. Specific methods for performance evaluation and related calculations are given.
3. True north calibration of the S band antenna was performed using the sun position. The S and X antenna's power patterns were measured utilizing the satellite as a signal source. Using the sun as a signal source, the G/T values in the direction of the sun's position between noon and sunset were measured, and the results were presented.

On the Kashiwa ground station, the following future developments are expected to be carried out:

- Enable the updating of satellite orbit data during satellite communication.
- Develop more optimized algorithms for real-time calibration of satellite positions.
- Identify why received solar signals attenuate at high elevation angles.
- Improve the G/T performance of the S receiving system by optimizing the hardware.

## Reference

- [1] Andy. Satellites Orbiting the Earth in 2022. < <https://www.pixalytics.com/satellites-in-2022/> >.
- [2] 倉原直美. インフラとしての地上局ネットワークの必要性. 会報「航空と宇宙」, 2018年12月第780号: 10-13.
- [3] A. J. Rolinski, et al. "The X-Y Antenna Mount for Data Acquisition from Satellites." IRE Transactions on Space Electronics and Telemetry, Vol. SET-8, No. 2, June 1962: 159-163.
- [4] J. R. Li. "Elementary analysis on vertex tracking of XY type antenna pedestal." Modern Electronics Technique, Vol. 11, April 2010: 21-23.
- [5] H. Yokotsuka, et al. "A Proposal on Antenna Alignment Calibration Method of a Receiving Ground Station for Earth Observation Satellite." IEEJ Transactions on Electronics Information and Systems, Vol. 126, No. 1, April 2006: 14-23.
- [6] 高木方隆. 人工衛星位置推算の実際(最終版). < <http://www.infra.kochi-tech.ac.jp/takagi/Geomatics/5Estimation2.pdf> >.
- [7] H. Rouzegar, et al. "Estimation of Doppler Curve for LEO Satellites." Wireless Pers Commun 108 (2019): 2195-2212.

- [8] Curtis, Howard D. (2019). *Orbital Mechanics for Engineering Students* (4th ed.).
- [9] A. A. Spiridonov, et al. "Small Satellite Orbit Determination Methods Based on the Doppler Measurements by Belarusian State University Ground Station." *IEEE Journal on Miniaturization for Air and Space Systems*, vol. 2, no. 2, June 2021: 59-66.
- [10] 吉田直子・他. フィーダリンク地球局アンテナ追尾制御装置. 通信総合研究所季報, Vol. 40, No. 2, June 1994: 195-201.
- [11] P. Rubio, et al. "Antenna Precise Pointing Calibration Using Low Cost DGPS." *International Telemetering Conference Proceedings*, vol. 54 (2018): 1-10.
- [12] Constantine A. Balanis. (2005). *Antenna theory: analysis and design* (3rd ed.).
- [13] 佐藤 奈穂子・他. 和歌山大学地上局パラボラアンテナの性能評価. 和歌山大学宇宙教育研究所紀要, Vol. 5, No. 2, March 2016: 11-15.
- [14] M. Morgan. "Determination of Earth Station Antenna G/T Using the Sun or the Moon as an RF Source." *32nd Annual AIAA/USU Conference on Small Satellites* (2018): 1-9.
- [15] S. Cakaj, et al. "Sun noise measurement at low Earth orbiting satellite ground station." *7th International Symposium ELMAR, Zadar, Croatia* (2005): 345-348.

[16] Christian Ho, et al. "Solar Brightness Temperature and Corresponding Antenna Noise Temperature at Microwave Frequencies." IPN Progress Report 42-175, November 2008.

[17] Christian Ho, et al. "Link Analysis of a Telecommunication System on Earth, in Geostationary Orbit, and at the Moon: Atmospheric Attenuation and Noise Temperature Effects." IPN Progress Report 42-168, February 2007.

[18] H. D. Qin, et al. "G/T Value Measurement of Satellite Communication Earth Station." Communications Technology, Vol. 49, No. 8, August 2016: 1078-1082.

[19] Wait, D. , et al. (1974). A study of the measurement of GT using Cassiopeia A.

[20] 年差を考慮した太陽位置の簡易計算. < [https://www.metds.co.jp/?smd\\_process\\_download=1&download\\_id=1781](https://www.metds.co.jp/?smd_process_download=1&download_id=1781) >.

[21] 太陽位置の計算. < [https://www.metds.co.jp/wp-content/uploads/2019/03/TE\\_Sun\\_Position\\_160401.pdf](https://www.metds.co.jp/wp-content/uploads/2019/03/TE_Sun_Position_160401.pdf) >.

[22] K. Yoshihide. "The Motion of a Close Earth Satellite." Astronomical Journal, Vol. 64, November 1959: 367-377.